ATLAS NOTE

ATL-COM-PHYS-2016-1674

28th June 2017

Draft version 0.5

Object selections for SM Higgs boson produced in association with a vector boson in which $H \to b\bar{b}$ and V decays leptonically with Run-2 data

Ahmadov, Faig[y], Argyropoulos, Spyridon[r], Arnold, Hannah[k], Amaral Coutinho, Yara[p], Sanchez Pineda, Arturo Rodolfo[q], Bell, Andrew Stuart[f], Benitez, Jose[r], Buzatu, Adrian[h], Calderini, Giovanni[v], Chan, Stephen Kam-wah[e], Chen, Chunhui[t], Buckley, Andrew[o], Buscher, Daniel[k], Delporte, Charles[l], De Lorenzi, Francesco[t], De Vivie De Regie, Jean-Baptiste[l], Dao, Valerio[a], Enari, Yuji[g], Francavilla, Paolo[v], Gargiulo, Simona[k], Gaycken, Goetz[n], Gray, Chloe[o], Grivaz, Jean-Francois[l], Hays, Jonathan Michael[j], Hesketh, Gavin Grant[f], Hobbs, John[a], Huth, John[e], Ishijima, Naoki[u], Kado, Marumi[l], Kato, Chikuma[g], Li, Changqiao[b], Li, Haifeng[a], Liu, Yanwen[b], Marchiori, Giovanni[v], Ma, Lianliang[i], Ma, Yanhui[i], Mario Jose da Cunha Sargedas de Sousa[x], Masubuchi, Tatsuya[g], Mallik, Usha[r], Mehta, Andrew[s], Montalbano, Alyssa[a], Morange, Nicolas[l], Moser, Brian[k], Pandini, Carlo Enrico[d], Piacquadio, Giacinto[a], Prell, Soeren[t], Robson, Aidan[o], Scanlon, Tim[f], Schopf, Elisabeth[n], Sekula, Stephen[w], Thompson, Paul[m], Tsybychev, Dmitri[a], Vergel Infante, Carlos Miguel[t], Wang, Song-Ming[h], Wang, Wei[h,z], Weiser, Christian[k], Yamaguchi, Yohei[c], Yang, Siqi[r], Yu, Jie[t]

[a]*Stony Brook University*
[b]*University of Science and Technology of China*
[c]*Tokyo Institute of Technology*
[d]*INFN Pisa and Universita' di Pisa, Dipartimento di Fisica*
[e]*Harvard University*
[f]*Department of Physics and Astronomy, University College London*
[g]*International Center for Elementary Particle Physics and Department of Physics, The University of Tokyo*
[h]*Academia Sinica, Taipei*
[i]*Shandong University (CN)*
[j]*Queen Mary University of London*
[k]*Albert-Ludwigs-Universitaet Freiburg*
[l]*LAL, Univ. Paris-Sud, IN2P3/CNRS, Universite Paris-Saclay*
[m]*University of Birmingham*
[n]*University of Bonn*
[o]*University of Glasgow, SUPA - School of Physics and Astronomy*
[p]*Universidade Federal do Rio De Janeiro, COPPE/EE/IF*
[q]*INFN Gruppo Collegato di Udine and Universita' di Udine, Dipartimento di Chimica, Fisica e Ambiente*
[r]*University of Iowa*
[s]*University of Liverpool*
[t]*Iowa State University*
[u]*Osaka University*
[v]*Laboratoire de Physique Nucleaire et de Hautes Energies (LPNHE), UPMC, Universite Paris-Diderot, CNRS/IN2P3*
[w]*Southern Methodist University, Department of Physics*
[x]*LIP and FCUL*
[y]*JINR*
[z]*Nanjing University, Department of Physics*

Abstract

This supporting note describes the object selections for the SM search for the Standard Model VH, with the Higgs boson decaying into $b\bar{b}$ and the V gauge boson (W or Z decaying leptonically), using proton-proton collisions data corresponding to an integrated luminosity of ~ 36.1 fb^{-1} at a $\sqrt{s} = 13$ TeV collected during 2015 and 2016 with the ATLAS at the LHC.

Contents

1. Updates

1.1. v0.0

First version of the note from the ICHEP 2016 note, with the bare minimum changes. It will be updated as we change the object definition for the publication 2017.

1.2. v0.1

Updates done:

- Removed Moriond 2016 and ICHEP 2016 appendices, both text and their many plots.
- Clarified this support note is used by objects also in SM VHcc, and BSM AZH and HVT, not only in the SM VHbb and BSM AZh mentioned before.
- Clarified this support note presents only the event preselection used to store the events in the CxAOD, and not the full event selection, described in the main support note of each analysis.
- CxAODFramework was a subsection in the Data/MC section. Made it its own section and placed right after the introduction.
- Improved readability in various sections by ensuring tables appear right after being mentioned in the text, by making text in equations with roman font, by adding spaces between a work and following parantheseis.
- Improved readability in Jet section by splitting the b-tagging subsection in direct and truth tagging subsubsections.
- Added brief summary of PtReco (while keep the b-jet energy correction summary and muon-in-jet correction), removed Regression, and references PtRece and Regression in detail from AZh Moriond 2016 object support note.

1.3. v0.2

Updates done:

- Added PtReco plot and $m_{b\bar{b}}$ comparison for the GSC, OneMu, PtReco and TruthWZ.
- Updated derivation selections including derivation trigger list.
- Updated 2015+2016 data PU plots.
- Added CP tools list associated to AnalysisBase 2.4.22.

1.4. v0.3

Updates done:

- Updated the 2016 MET trigger studies.
- Updated the lepton trigger selection in 2-lepton.
- A few sentences on the plans for the tighter isolation that is currently being studied.
- Finalization of 1-lepton trigger strategy.
- Updated the luminosity and pile-up uncertainties.
- AnalysisBase release updated to 2.4.26.
- Lepton selections updated.
- Updated the el/mu for b-jet energy corrections and the jet selections.

1.5. v0.4

Updates done:

- State that we are using CxAOD v28 with latest CP recommendation.
- AnalysisBase release updated to 2.4.27.
- ttbar sample updated to PP8.
- 1 lepton new isolation updated.
- *b*-tagging SF described in a subsubsection.

1.6. v0.5

Updates done:

- Improved the description of lepton-in-jet counts of how often el, mu, hadronic.
- Clarified at the beginning of the b-jet energy corrections that we use muon-in-jet + PtReco.
- Added a subsection of the Z+b data vs MC, as argument that no systematic is used for PtReco.
- Updated the description for the JES systematics (19 -> 21).
- Updated integrated luminosity from 36.5 to 36.1 to be consistent with the main support note.
- Updated *b*-tagging systematics. Table 14 to only show the chosen operatin point (medium), and for this one replace the c-tagging reduction scheme from 4 to 3.
- Updated Overlap removal description based on Kristian Gregersen's nice clarifications.
- Updated to the latest *b*-tagging CDI: 2016-20_7-13TeV-MC15-CDI-2017-06-07_v2.root
- Corrected description of d_0 and z_0 relative to the beam line (BL).

2. Introduction

In LHC Run-1 a Higgs boson was discovered by the ATLAS and CMS collaboration [1, 2]. Since discovery of the new boson the ATLAS and CMS experiments has precisely measured the Higgs boson properties. The measured Higgs boson mass combined ATLAS and CMS results is 125.09 ± 0.24 GeV [3]. The ATLAS and CMS experiments recently combined the measurement of the Higgs boson production and decay rates [4]. The significant Higgs boson signals decaying into a pair of photons, a pair of Z and W bosons and a pair of τ leptons were observed in Run-1. However the observed significance on the decay to a pair of bottom quarks is 2.6 σ (expected significance 3.7 σ) in spite of largest decay branching ratio (58%). Therefore an observation of the decay to a pair of b quarks is one of important milestones in Higgs boson property measurement in Run-2. The VH production process is the most sensitive process to search for $H \to b\bar{b}$ decay mode, thanks to the associated vector boson, which is essential to reduce multi-jet backgrounds.

Based on Run-1 analysis [5], we update the search for the Higgs boson decaying to a pair of b quark with the Higgs produced in association with a vector boson, using ~ 36.5 fb^{-1} data at $\sqrt{s} = 13$ TeV delivered by the LHC in 2015 and 2016. The analysis is performed in three categories for events containing zero, one or two charged leptons. This targets three channels of Higgs production ($ZH \to \nu\nu b\bar{b}$, $WH \to \ell\nu b\bar{b}$ and $ZH \to \ell\ell b\bar{b}$), where ℓ indicates an electron or a muon. In the final state of the three channels one or two leptons and/or missing transverse energy and two b-jets would be observed. These object definitions and events selections are important to maximize search sensitivity. Another SM VH search performed is that where the Higgs boson decays to charm quark pairs with a BR of about 3%. The analyis is very similar to the $VH(b\bar{b})$ one, except replacing the b-tagging requirements with orthogonal c-tagging one.

In addition to the Standard Model Higgs boson analysis, VH signatures have also important role for the beyond the Standard Model Higgs search [6]. A simple extension of the SM Higgs sector is given by the addition of a second complex Higgs doublet, giving rise to five Higgs bosons: two CP-even scalar fields h and H, one pseudo-scalar A that is CP-odd and two charged Higgs bosons (H^+ and H^-). The h boson has properties very similer to those predicted by the SM and is thought to be the 125 GeV Higgs boson. The H boson is thought to have a larger mass than 125 GeV. These 2HDM extensions have been predicted by many beyond Standard Models (such as SUSY, or electroweak baryogenesis). We also search for $A \to Zh$ and $A \to ZH$, (with either h or H decaying to $b\bar{b}$), and the Z boson decaying to two charged leptons, since the strategy of analyses is similar to the Standard Model search. We also search for a BSM process of a HVT particle decaying to a W boson and an h boson.

This supporting note describes object selections and event preselections for the CxAOD production used in common for the SM and BSM VH searches described above, due to their very similar signatures. The full event selection, the background modeling, fit strategy and main results are analysis specific and described in other supporting documents of the respective analyses. Section 4 describes the collision data collected in Run-2 and Monte Carlo (MC) used in this analysis, and also describes the analysis framework using DxAOD and CxAOD. Section 5 describes triggers choices for each channel. Section 6 describes the charged lepton (electron and muon) object definition. Section 7 describes jet collection and b-tagging. Section 8 briefly notes our object overlap removal strategy. Section 9 describes the missing transverse momentum definition. Section 10 discusses the event preselection for events to be stored in the CxAOD. Section 11 summarizes the experimental systematic uncertainties due to data conditions (luminosity, triggers) and object reconstruction. Signal and background modelling systematics are described in the modelling support note.

3. CxAOD Framework

Hbb group decided to provide a shared framework for Run-2 users, called the CxAOD Framework in order to apply basic object and event selection, and to use the combined performance(CP) recommendations. It is a two steps level set of codes: the CxAODMaker and the CXAODReader, as illustrated in Figure 1.

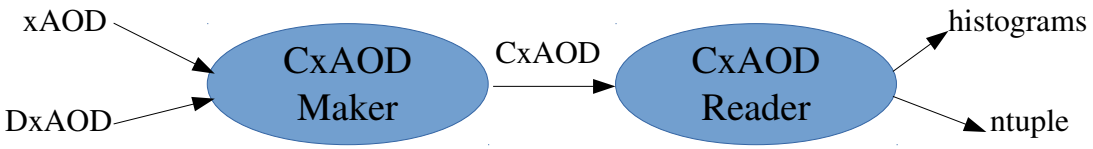

Figure 1: Overview of the Hbb CxAOD Framework.

3.1. CxAODMaker

This step can use as input xAOD or derivation format DxAOD files. Several operations are done at this step: lepton selection (0 or 1 or 2 leptons depending on the analysis), jet pre-selection, object calibration (leptons, jets, $E_{\mathrm{T}}^{\mathrm{miss}}$), the computation of the overlap removal, the computation of the systematics affecting the kinematics and the computation of some corrections (pile-up, lepton trigger SF). In the end, each channel has a specific set of calibrated xAOD files, called CxAOD files.

3.2. CxAODReader

This step takes as an input the CxAOD files produced in previous level and produces very fast physics studies, producing inputs to the final fit. At this level we have the possiblity to use directly information stored or re-compute most of them (calibrations, overlap removal, pile-up) and tighten the lepton or jet selection. Then we also apply the optimized analysis selections and all the needed corrections as luminosity, cross-section, *b*-tagging SF. Note that the Run-1 `CorrAndSyst` has been updated to be used in this framework. Finally, it is possible to store ntuples (to perform training of multivariate analysis based) and histograms (for final fit).

Selection	Value
HIGG5D1	
Trigger	$E_{\mathrm{T}}^{\mathrm{miss}}$ triggers (Appendix B) HLT_j80_xe80_dphi1_L1J40_DPHI-J20XE50 HLT_j80_xe80_dphi1_L1J40_DPHI-J20s2XE50 HLT_j100_xe80_L1J40_DPHI-J20XE50 HLT_j100_xe80_L1J40_DPHI-J20s2XE50 HLT_noalg_L1J400 HLT_g120_loose HLT_g140_loose HLT_g160_loose
Jets	count((AntiKt4EMTopoJets.pt > 15.0*GeV) && (|AntiKt4EMTopoJets.eta| < 2.6))) > 0

Table 1: List of selection criteria for the HIGG5D1 DxAODs used in the analyses.

Selection	Value
HIGG5D2	
Trigger	$E_{\mathrm{T}}^{\mathrm{miss}}$ triggers and single lepton triggers (Appendix B) HLT_e15_lhtight_ivarloose_3j20_L1EM13VH_3J20 HLT_mu14_ivarloose_3j20_L1MU10_3J20 HLT_j80_xe80_dphi1_L1J40_DPHI-J20XE50 HLT_j80_xe80_dphi1_L1J40_DPHI-J20s2XE50 HLT_j100_xe80_L1J40_DPHI-J20XE50 HLT_j100_xe80_L1J40_DPHI-J20s2XE50 HLT_noalg_L1J400
Jets	count((AntiKt4EMTopoJets.pt > 15.0*GeV) && (|AntiKt4EMTopoJets.eta| < 2.6))) > 0
Leptons	count((Muons.pt > 20.0*GeV) && (|Muons.eta| < 2.6) && (DFCommonGoodMuon)) + count((Electrons.pt > 20.0*GeV) && (|Electrons.eta| < 2.6) && (DFCommonElectronsLHLoose)) > 0

Table 2: List of selection criteria for the HIGG5D2 DxAODs used in the analyses.

4. Data and MC

Data and Monte Carlo samples are originally in a large, comprehensive format known as xAOD. These samples are reduced in size on a per-analysis basis. These "derived" samples, or DxAODs, are produced centrally with the expressed goals of reducing sample sizes. The derivations relevant to this analysis are HIGG5D1 for the 0-lepton channel, HIGG5D2 for the 1-lepton channel, and HIGG2D4 for the 2-lepton channel. The list of selection criteria for these derivations are given in Tables 1, 2, and 3. In this analysis, data and MC DxAODs are further produced through CxAOD Framework version 28 with AnalysisBase 2.4.27 and with the latest CP recommendation (more details about CP tools associated to the AnalysisBase can be found on Appendix A).

Selection	Value
HIGG2D4	
Trigger	L1_EM.* or L1_2EM.* or L1_MU.* or L1_2MU.*
Jets	count((AntiKt4EMTopoJets.pt > 15.0*GeV) && (|AntiKt4EMTopoJets.eta| < 2.6))) > 0
Leptons	(count((Muons.pt > 6.0*GeV) && (DFCommonMuonsPreselection)) + count((Electrons.pt > 6.0*GeV) && (DFCommonElectronsLHVeryLoose)) > 1) and m_{ll} > 5.0*GeV

Table 3: List of selection criteria for the HIGG2D4 DxAODs used in the analyses.

4.1. Data

The datasets used in this analysis include only pp collision data recorded in stable beam conditions and with all relevant sub-detectors providing high-quality data. The integrated luminosity in our datasets is 36.5 fb^{-1} at a center-of-mass energy $\sqrt{s}$ = 13 TeV. High data quality is maintained by pruning events through a Good Runs List (GRL [7]) tool provided by the ATLAS Data Quality Group. This tool uses data-quality status flags from specific areas of the detector to determine if an event within a given luminosity block is suitable for physics analysis. In addition to using a GRL, events corrupted from bad TileCal and LAr noise bursts are removed as well. The GRL is necessary to determine the correct amount of luminosity processed. A Luminosity Calculator is also provided that computes the total integrated luminosity for a given GRL XML file. Data event weights may also be adjusted by an official pileup (PU) reweighting tool [8] to account for trigger prescales. A more accurate estimate of the mean number of interactions per crossing μ can also be obtained from this tool.

4.2. MC

Monte Carlo (MC) events are used to compare expected yields of background and signal processes. The various processes along with their respective generators are given in Table 4.

Each MC event must be reweighted in order to make accurate comparisons to data. This involves rescaling the total MC yield to the measured luminosity, weighting each MC event by a factor that accounts for the differences in simulated and actual detector conditions (PU weight [9]), and MC generator weights that are often found in physics processes where different amplitudes contribute to a given process and account for possible interference. Samples with interference may have events with negative weights, which are essential in correctly representing physical distributions affected by the interference process. The rescaling of the total MC yield is straightforward once the luminosity is obtained from the Luminosity Calculator. The PU reweighting is accomplished through an official tool that provides corrections of MC events that account for differences in pileup distributions between MC and data shown in Figure 2.

Flavor tagging requires the use of scale factors (SF) that modify the MC event weight. These SFs depend on the MC generator, jet p_{T}, η, and flavor label. They are provided by the recommended BTaggingEfficiency CP tool.

Process	Generator
SM Signal	
$q\bar{q} \to ZH \to \nu\bar{\nu}b\bar{b}/llb\bar{b}$	Pythia 8 + EvtGen
$gg \to ZH \to \nu\bar{\nu}b\bar{b}/llb\bar{b}$	Powheg + Pythia 8 + EvtGen
$q\bar{q} \to WH \to l\bar{\nu}b\bar{b}$	Pythia 8 + EvtGen
ggA $\to ZH$ Signal	
$llbb$, $\nu\nu bb$, all masses	MadGraph + Pythia 8 + EvtGen
b$\bar{b}$A $\to ZH$ Signal	
$llbb$, $\nu\nu bb$, all masses	aMC@NLO + Pythia 8 + EvtGen
HVT Signal	
$qqbb$, $l\nu bb$, $llbb$, $\nu\nu qq$, all masses	MadGraph + Pythia 8
QCD	
multi-jet	Pythia 8 + EvtGen
Vector boson + jets	
$W \to l\bar{\nu}$ + jets	Sherpa
$Z \to l\bar{l}$ + jets	Sherpa
$Z \to \nu\bar{\nu}$ + jets	Sherpa
Top-quark	
$t\bar{t}$	Powheg + Pythia 8 + EvtGen
single top $t-$channel	Powheg + Pythia 6 + EvtGen
single top $s-$channel	Powheg + Pythia 6 + EvtGen
single top $Wt-$channel	Powheg + Pythia 6 + EvtGen
Diboson	
WW	Sherpa
WZ	Sherpa
ZZ	Sherpa

Table 4: List of signal and background samples for the analyses.

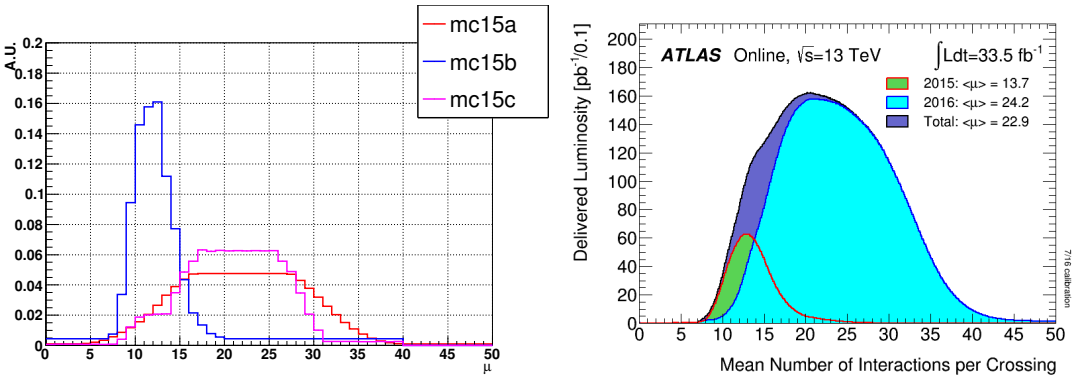

Figure 2: Comparison of average pileup (mu or μ, plotted in arbitrary units) between and MC15a, MC15b and MC15c(left) and the corrected luminosity for 2015+2016 data(right).

5. Trigger Selection

Events in the 1- and 2-lepton channels are primarily selected using the unprescaled single lepton triggers, except that the muon channel in 1-lepton analysis uses missing transverse energy ($E_{\mathrm{T}}^{\mathrm{miss}}$) trigger. Events in the 0-lepton channel are selected using triggers based on the $E_{\mathrm{T}}^{\mathrm{miss}}$. The thresholds used are the lowest defined for the Run-2 luminosity in [10]. As the trigger used vary from each data period, period-dependent SFs are applied according to the corresponding trigger.

The summary of trigger items used can be found in Tables 5 and 6. The part dedicated to systematics can be found in Sec 11.2. In order to handle properly triggers in simulation, we use the random run number proivded by pile-up reweighting tool to define if the event is associated to 2015 or 2016 data and then the associated set of triggers/corrections/systematics are used.

0 lep	1 lep	2 lep
HLT_xe70	HLT_xe70 HLT_e24_lhmedium_L1EM20VH OR HLT_e60_lhmedium OR HLT_e120_lhloose	HLT_mu20_iloose_L1MU15 OR HLT_mu40 HLT_e24_lhmedium_L1EM20VH OR HLT_e60_lhmedium OR HLT_e120_lhloose

Table 5: Summary table of triggers used in 2015 Data.

period	0 lep	1 lep	2 lep
A	HLT_xe90_mht_L1XE50	HLT_xe90_mht_L1XE50 HLT_e26_lhtight_nod0_ivarloose OR HLT_e60_lhmedium_nod0 OR HLT_e60_medium OR HLT_e140_lhloose_nod0	HLT_mu24_ilosse(data) HLT_mu24_ilosse_L1MU15(MC) OR HLT_mu40 HLT_e26_lhtight_nod0_ivarloose OR HLT_e60_lhmedium_nod0 OR HLT_e60_medium OR HLT_e140_lhloose_nod0
B-D3	HLT_xe90_mht_L1XE50	HLT_xe90_mht_L1XE50 HLT_e26_lhtight_nod0_ivarloose OR HLT_e60_lhmedium_nod0 OR HLT_e60_medium OR HLT_e140_lhloose_nod0	HLT_mu24_ivarmedium OR HLT_mu50 HLT_e26_lhtight_nod0_ivarloose OR HLT_e60_lhmedium_nod0 OR HLT_e60_medium OR HLT_e140_lhloose_nod0
D4-E3	HLT_xe110_mht_L1XE50	HLT_xe110_mht_L1XE50 HLT_e26_lhtight_nod0_ivarloose OR HLT_e60_lhmedium_nod0 OR HLT_e60_medium OR HLT_e140_lhloose_nod0	HLT_mu24_ivarmedium OR HLT_mu50 HLT_e26_lhtight_nod0_ivarloose OR HLT_e60_lhmedium_nod0 OR HLT_e60_medium OR HLT_e140_lhloose_nod0
≥F1	HLT_xe110_mht_L1XE50	HLT_xe110_mht_L1XE50 HLT_e26_lhtight_nod0_ivarloose OR HLT_e60_lhmedium_nod0 OR HLT_e60_medium OR HLT_e140_lhloose_nod0	HLT_mu26_ivarmedium OR HLT_mu50 HLT_e26_lhtight_nod0_ivarloose OR HLT_e60_lhmedium_nod0 OR HLT_e60_medium OR HLT_e140_lhloose_nod0

Table 6: Summary table of triggers used in 2016 Data.

.

5.1. Trigger for 0 lepton analysis ($E_{\mathrm{T}}^{\mathrm{miss}}$ trigger)

The trigger chains we use are non-prescaled $E_{\mathrm{T}}^{\mathrm{miss}}$ trigger : `HLT_xe70` which is seeded with `L1_XE50` for 2015 Data and `HLT_xe90_mht_L1XE50` or `HLT_xe110_mht_L1XE50` for 2016 Data. To maximize the performance of the analysis, part of the phase space is in a region where the trigger is not completely efficient. It's very important to study the trigger efficiency in this region to check and understand the behavior of data and simulation response to the efficiency. In this study, the trigger efficiency is measured in both data and simulation, and are compared to determine the data driven scale factor to correct the simulation if there is any difference between them [11],[12].

5.1.1. Samples and Physics Processes for Efficiency Measurements

The final state signature of the $\nu\nu qq$ analysis consists of $E_{\mathrm{T}}^{\mathrm{miss}}$ plus jets. Thus we should select physics processes that have similar final state signature to measure the $E_{\mathrm{T}}^{\mathrm{miss}}$ trigger efficiency. A muon deposits minimum energy in the calorimeter as it traverses through it. At the trigger level the $E_{\mathrm{T}}^{\mathrm{miss}}$ is determined only based on the energy measured in the calorimeter. Thus the $W(\mu,\nu)$+jets process provides a topology at the trigger level that is very similar to the $E_{\mathrm{T}}^{\mathrm{miss}}$ plus jets signature of the $\nu\nu qq$ final state. In this study we use the $W(\mu,\nu)$+jets process to derive the scale factor. As the process of semi-leptonic $t\bar{t}$ which decay into one muon has a similar behavior with $W(\mu,\nu)$+jets in the trigger level, this process are also studied as a comparison.

5.1.2. Trigger Efficiency Measurements

The measurements are performed on the 13TeV 25ns data and simulated samples. Events from 2015 are collected with `HLT_mu20_iloose_L1MU15` OR `HLT_mu50` trigger and events from 2016 are collected with the loested un-prescaled muon trigger listed in [10]. These muon triggers are orthogonal to the $E_{\mathrm{T}}^{\mathrm{miss}}$ trigger, and thus do not bias the $E_{\mathrm{T}}^{\mathrm{miss}}$ trigger efficiency measurement.

The $E_{\mathrm{T}}^{\mathrm{miss}}$ trigger efficiency has an obvious large dependency on the offline $E_{\mathrm{T}}^{\mathrm{miss}}$ `MET_TST`. In `MET_TST` the contributions from the presence of muons are included in the $E_{\mathrm{T}}^{\mathrm{miss}}$ determination. To mimic the $E_{\mathrm{T}}^{\mathrm{miss}}$ plus jets topology from $W(\mu,\nu)$+jets events, and also to be consistent with the $E_{\mathrm{T}}^{\mathrm{miss}}$ at the trigger level, we re-compute the offline $E_{\mathrm{T}}^{\mathrm{miss}}$ by removing the muon's contribution in `MET_TST` ($E_{\mathrm{T}}^{\mathrm{miss,no\_mu}}$).

The $W(\mu,\nu)$+jets events are selected with these selection cuts:

- pass single muon trigger
- pass GRL (for data events) of 2015(2016)
- re-weight pile-up for simulated events to 2015(2016) data
- exactly one muon candidate passing the Medium or Tight muon ID criteria with $p_{\mathrm{T}}(\mu) > 27$ GeV, and passing the isLooseTrackOnly isolation cut.
- two or three selected jets and at least two signal jets. Similar calibration corrections are applied to the jets as in the $\nu\nu qq$ analysis.
- Transverse momentum of leading signal jet $p_{\mathrm{T}} > 45$ GeV

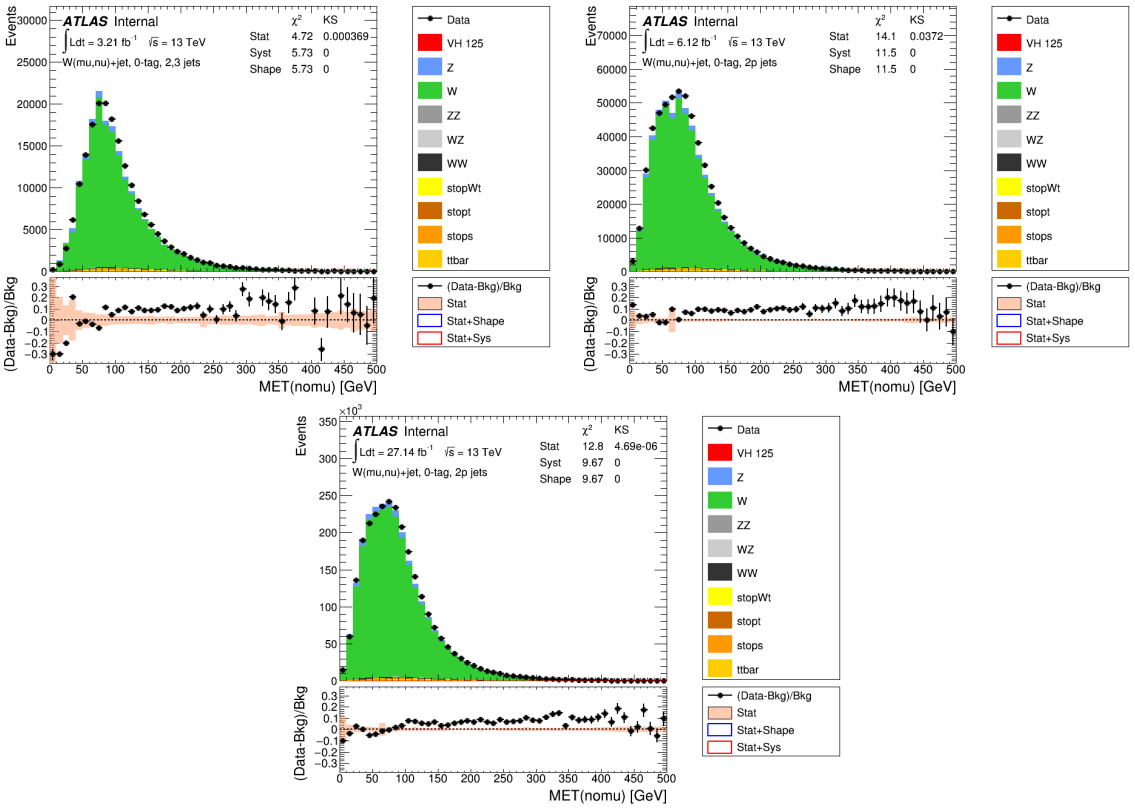

Figure 3: Distribution of $E_{\mathrm{T}}^{\mathrm{miss,no\_mu}}$ for 2015 (left) and 2016 data priod A-D3 (right) and 2016 data period D4-F11 (bottom) $W(\mu,\nu)$+jets events after the selection.

- missing transverse momentum $MPT > 30$ GeV.
- missing transverse energy $E_{\mathrm{T}}^{\mathrm{miss}} > 30$ GeV.
- b-jet veto to reject $t\bar{t}$ background.

The selection for $t\bar{t}$ events are almost same with $W(\mu,\nu)$+jets events except that we require more than three jets and at least one jet is b-tagged.

Figure 3 and Figure 4 show the distribution of $E_{\mathrm{T}}^{\mathrm{miss,no\_mu}}$ for 2015 and 2016 sample after the selection.

The $E_{\mathrm{T}}^{\mathrm{miss}}$ trigger efficiency is defined as

$$\text{Efficiency} = \frac{\text{\# Events passed selection and } \mathrm{E_T^{miss}} \text{ trigger}}{\text{\# Events passed selection}}. \quad (1)$$

and the measured $E_{\mathrm{T}}^{\mathrm{miss}}$ trigger efficiencies as function of offline $E_{\mathrm{T}}^{\mathrm{miss}}$ ($E_{\mathrm{T}}^{\mathrm{miss,no\_mu}}$) for $W(\mu,\nu)$+jets events are shown in Figure 5

5.1.3. Dependencies of $E_{\mathrm{T}}^{\mathrm{miss}}$ Trigger Efficiency on Kinematic Variables

We expect a clear dependence between the efficiency and the offline $E_{\mathrm{T}}^{\mathrm{miss}}$, so the dependencies of the $E_{\mathrm{T}}^{\mathrm{miss}}$ trigger efficiency on other kinematic variables have been studied. The `SumPt`, p_{T} (J1) and p_{T} (J2)

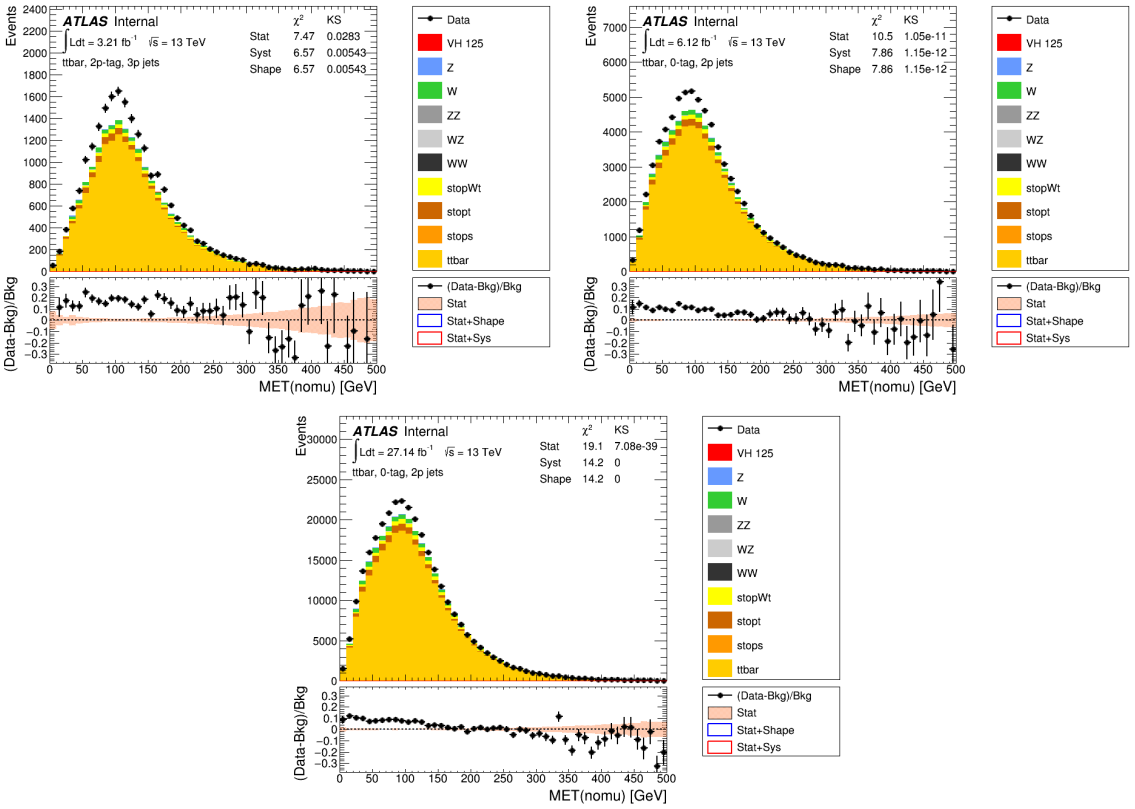

Figure 4: Distribution of $E_{\mathrm{T}}^{\mathrm{miss,no\_mu}}$ for 2015 (left) and 2016 data period A-D3 (right) and 2016 data period D4-F11 (bottom) $t\bar{t}$ events after the selection.

shows significant correlations with the $E_{\mathrm{T}}^{\mathrm{miss}}$ trigger efficiency, where the `SumPt` is the scalar sum p_{T} of the selected signal jets. The definition of `SumPt` is

$$\texttt{SumPt} = p_{\mathrm{T}}^{\mathrm{j1}} + p_{\mathrm{T}}^{\mathrm{j2}} \quad \text{for events with 2 jets.} \tag{2}$$

$$\texttt{SumPt} = p_{\mathrm{T}}^{\mathrm{j1}} + p_{\mathrm{T}}^{\mathrm{j2}} + p_{\mathrm{T}}^{\mathrm{j3}} \quad \text{for events with 3 or more jets.} \tag{3}$$

Since `SumPt` is highly correlated to p_{T} (j1) and p_{T} (J2), the trigger study only considers `SumPt` dependency. Figure 6 shows the $E_{\mathrm{T}}^{\mathrm{miss}}$ trigger efficiencies as function of offline $E_{\mathrm{T}}^{\mathrm{miss}}$ ($E_{\mathrm{T}}^{\mathrm{miss,no\_mu}}$) and `SumPt`, measured for $W(\mu, \nu)$+jets events. The plots highlight an interdependence of the trigger efficiency between `SumPt` and offline $E_{\mathrm{T}}^{\mathrm{miss}}$, which means that the $E_{\mathrm{T}}^{\mathrm{miss}}$ trigger efficiency as function of offline $E_{\mathrm{T}}^{\mathrm{miss}}$ will have a different turn-on efficiency curves for low `SumPt` region and high `SumPt` region. Thus one also needs to check whether the $E_{\mathrm{T}}^{\mathrm{miss}}$ trigger efficiency as function of offline $E_{\mathrm{T}}^{\mathrm{miss}}$ behaves in the same way in data as in the simulation. Figure 7 shows the ratio of $E_{\mathrm{T}}^{\mathrm{miss}}$ trigger efficiencies for data and simulation with respect to the offline $E_{\mathrm{T}}^{\mathrm{miss}}$ and `SumPt`. This plots indicates that the difference behavior of data and simulation on trigger efficiency has a correlation with `SumPt`. Thus we adopted an extra cut on `SumPt` to avoid the bias induced by this correlation. For the 2-jets case, an 120GeV cut on `SumPt` is applied, while the cut for 3 or more jets events is 150GeV. The effect on sensitivity of this `SumPt` cut has also been studied, and the result turned out that the effect is negligible.

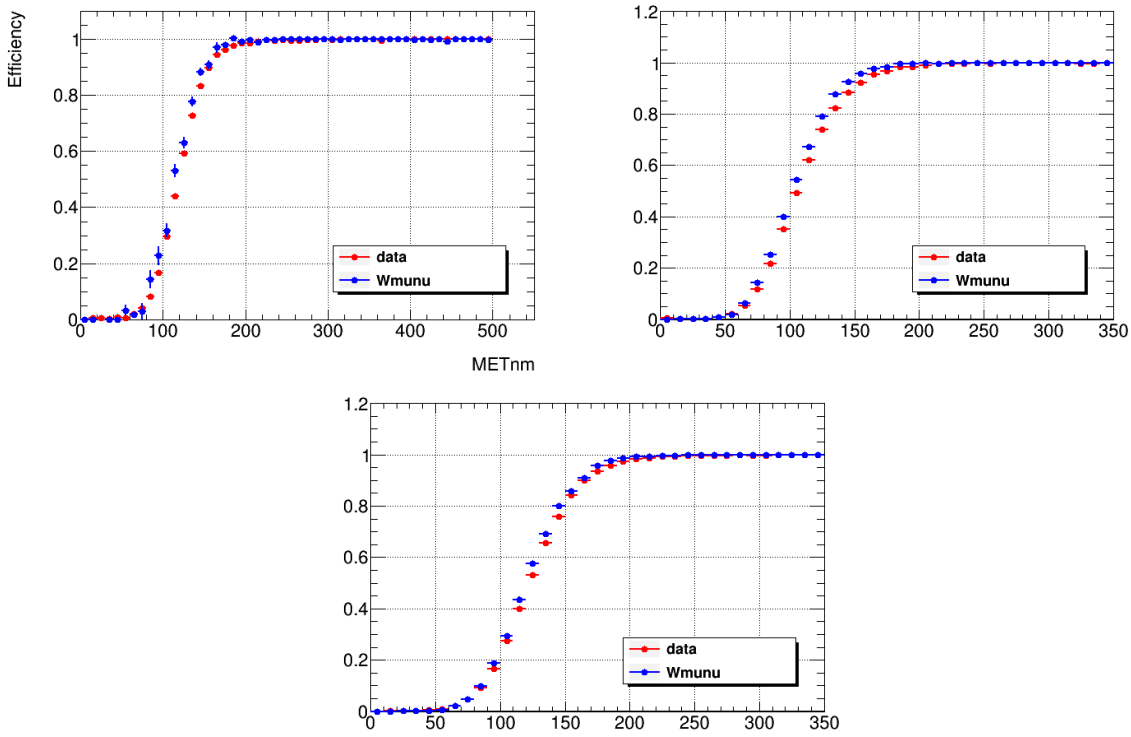

Figure 5: Measured $E_{\mathrm{T}}^{\mathrm{miss}}$ trigger efficiencies as function of offline $E_{\mathrm{T}}^{\mathrm{miss}}$ for $W(\mu,\nu)$+jets events for `HLT_xe70` (left), `HLT_xe90_mht_L1XE50` (right) and `HLT_xe110_mht_L1XE50` (bottom).

5.1.4. Data driven scale factor of $E_{\mathrm{T}}^{\mathrm{miss}}$ Trigger

From the $E_{\mathrm{T}}^{\mathrm{miss}}$ trigger efficiency measured above, one can take the ratio of the efficiencies for data and simulation to get the data driven scale factor (SF). The definition of the SF is given by Equation

$$\mathrm{SF} = \frac{\mathrm{Turn-On}^{\mathrm{Data}}_{\mathrm{W}(\mu,\nu)+\mathrm{jets}}}{\mathrm{Turn-On}^{\mathrm{MC}}_{W(\mu,\nu)+\mathrm{jets}}}. \tag{4}$$

With the reduction of the non-trivial dependence of the trigger efficiency by other variables, as described in previous sections, the $E_{\mathrm{T}}^{\mathrm{miss}}$ trigger scale factor has a dependence only on the reconstructed $E_{\mathrm{T}}^{\mathrm{miss}}$. The calculated scale factor has been plotted as a function of the offline $E_{\mathrm{T}}^{\mathrm{miss}}$, and been fitted using the error function

$$\mathrm{SF} \;=\; 0.5 \times \left(1 + Erf\left(\frac{E_{\mathrm{T}}^{\mathrm{miss}} - p0}{\sqrt{2}\times p1}\right)\right). \tag{5}$$

where the p0 and p1 represent the threshold and the width of the fit function. The fit range for the scale factor is 100-250 GeV. The results for different $E_{\mathrm{T}}^{\mathrm{miss}}$ triggers are shown in Figure 8.

5.1.5. Uncertainties of the scale factor

In the scale factor calculation, 1σ confidence interval of the fit function is taken as the statistical error (`METTrigStat`), which is already shown in Figure 8. And we also studied the semi-leptonic $t\bar{t}$ events

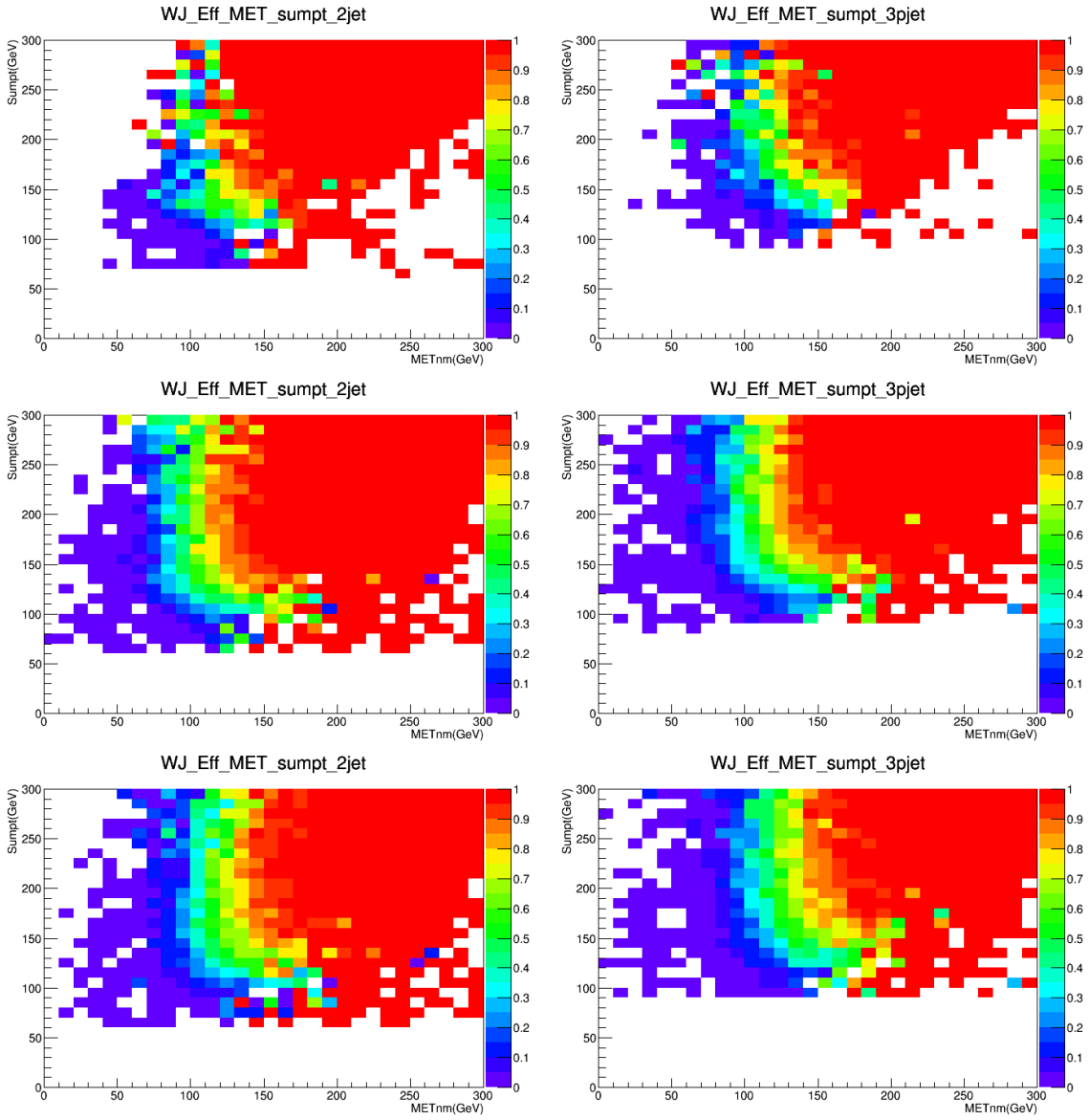

Figure 6: $E_{\mathrm{T}}^{\mathrm{miss}}$ trigger efficiency as function of $E_{\mathrm{T}}^{\mathrm{miss}}$ and `SumPt` for $W(\mu,\nu)$+jets simulation events. Left: njet = 2 events, right: njet $\geq$ 3 events (njet is the number of selected jets). Top: `HLT_xe70`, middle: `HLT_xe90_mht_L1XE50`, bottom: `HLT_xe110_mht_L1XE50`.

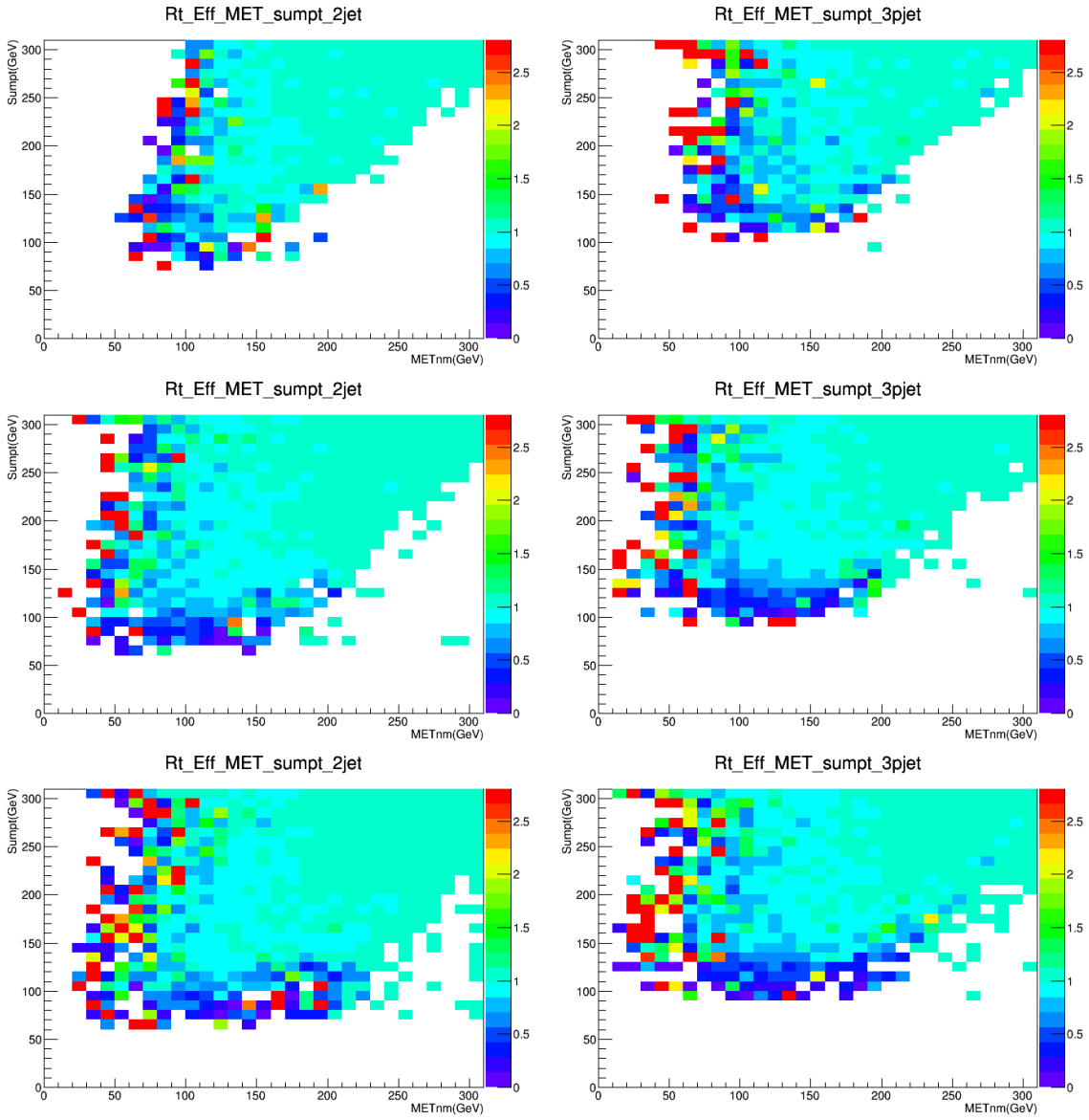

Figure 7: The ratio of the $E_{\mathrm{T}}^{\mathrm{miss}}$ trigger efficiencies for data and simulation, with respect to $E_{\mathrm{T}}^{\mathrm{miss}}$ and `SumPt` for $W(\mu,\nu)$+jets events. Left: njet = 2 events, Right: njet $\geq$ 3 events (njet is the number of selected jets). Top: `HLT_xe70`, middle: `HLT_xe90_mht_L1XE50`, bottom: `HLT_xe110_mht_L1XE50`.

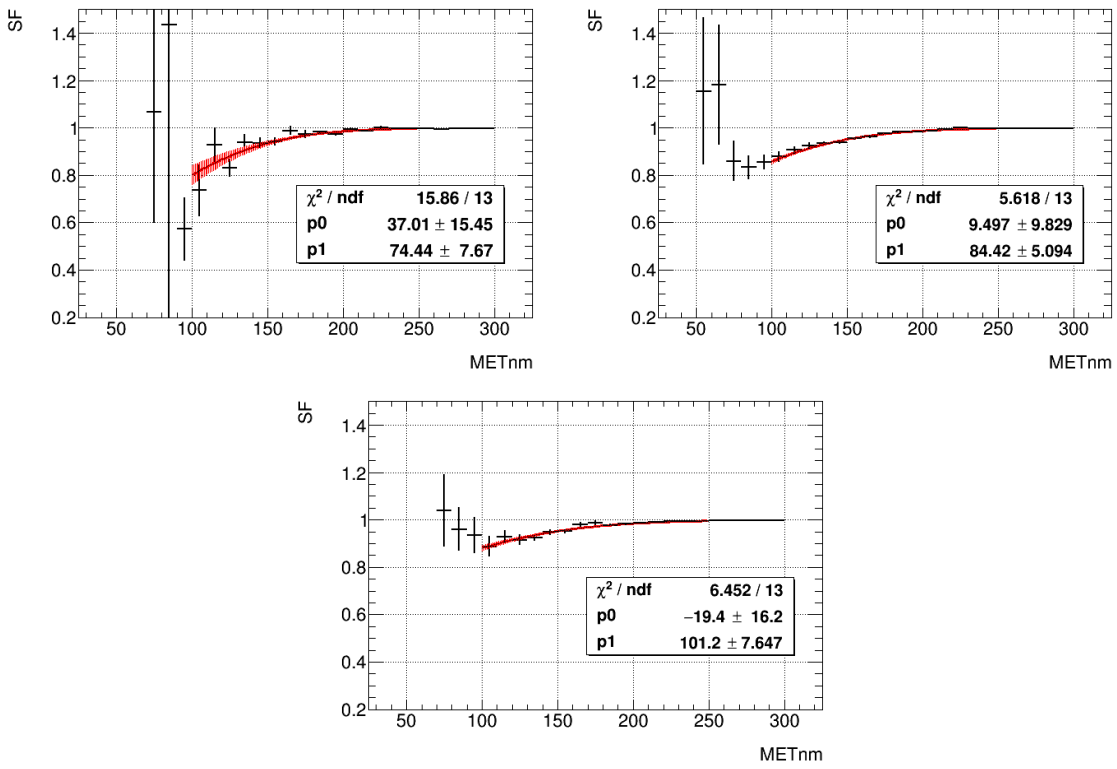

Figure 8: Calculated $E_{\mathrm{T}}^{\mathrm{miss}}$ trigger scale factor from the Sherpa $W(\mu,\nu)$+jets events for `HLT_xe70` (left), `HLT_xe90_mht_L1XE50` (right) and `HLT_xe110_mht_L1XE50` (bottom). The 1σ confidence interval of the fit result is shown.

as a comparison, result shown in Figure 9. The comparison of the scale factors for $W(\mu,\nu)$+jets and $t\bar{t}$ shows a discrepancy approximately 2% when $E_{\mathrm{T}}^{\mathrm{miss}} > 150$GeV. The discrepancy is then considered as the systematic uncertainty in the analysis (`METTrigTop`).

5.2. Trigger for 1/2-lepton analysis (Lepton and $E_{\mathrm{T}}^{\mathrm{miss}}$ triggers)

5.2.1. Recommended chains

The final state signature of the $lvqq$ analysis consists of one lepton plus $E_{\mathrm{T}}^{\mathrm{miss}}$ plus jets, and the $llqq$ analysis consists of two leptons plus jets. Electrons and muons channels are considered and the trigger strategy for these channels is based on lepton triggers objects mainly.

For analysis containing muons in the final state, the following triggers are used for 2015 Data : `HLT_mu20_iloose_L1MU1` OR `HLT_mu40`. It is composed of a trigger with low muon p_{T} threshold with a track isolation to deal with LHC pile-up conditions, and a higher muon p_{T} threshold wihtout any isolation requirement to compensate the slight inefficiency cuts. For 2016 Data, different triggers can be accessed depending on luminosity conditions. The detail of various triggers used in 2015 and 2016 datasets can be found in Tables 5 and 6.

Due to inefficiencies in single muon triggers, the usage of $E_{\mathrm{T}}^{\mathrm{miss}}$ triggers in one lepton (muon events) is studied. The study [13] [14] has defined how much we can recover by adding $E_{\mathrm{T}}^{\mathrm{miss}}$ trigger in lepton events

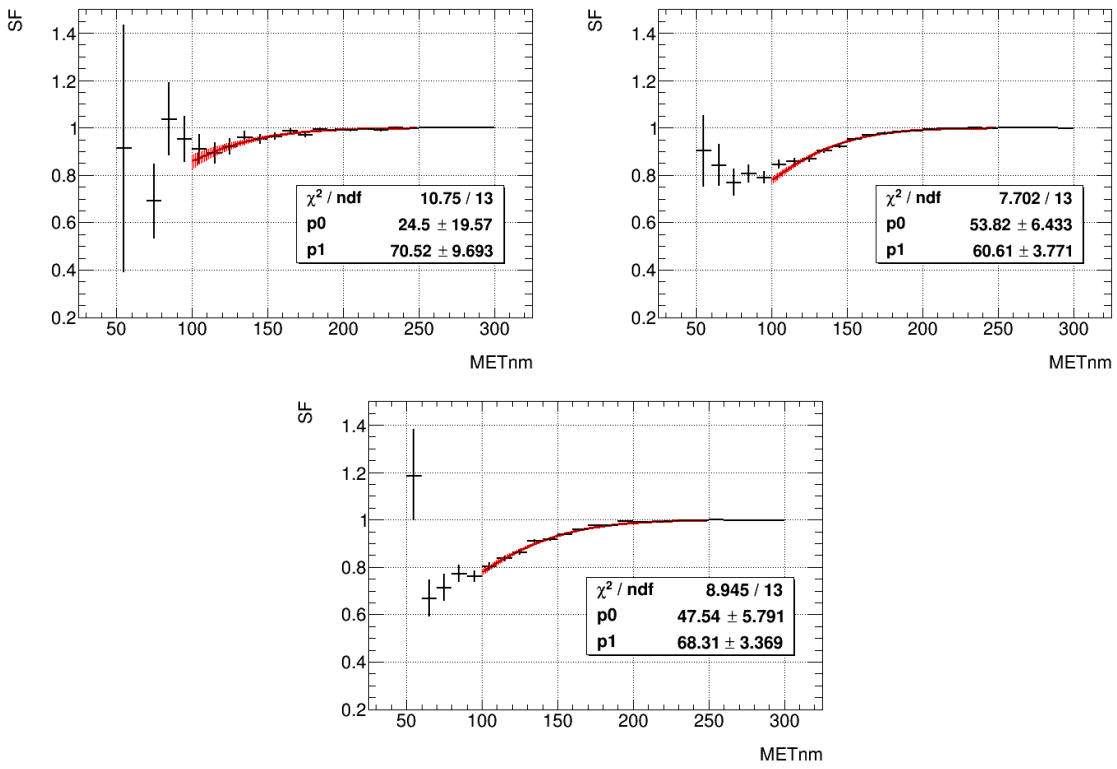

Figure 9: Calculated $E_{\mathrm{T}}^{\mathrm{miss}}$ trigger scale factor from the $t\bar{t}$ events for `HLT_xe70` (left), `HLT_xe90_mht_L1XE50` (right) and `HLT_xe110_mht_L1XE50` (bottom). The 1σ confidence interval of the fit result are shown.

of the one lepton channel. It has benn decided to use the similar $E_{\mathrm{T}}^{\mathrm{miss}}$ trigger as 0 lepton analysis for events with W boson in 1 lepton analysis.

For electron analysis final state, the following OR of triggers are used for 2015 Data : `HLT_e24_lhmedium_L1EM20VH` OR `HLT_e60_lhmedium` OR `HLT_e120_lhloose`. Both `HLT_e60_lhmedium` and `HLT_e120_lhloose` are seeded by `L1_EM22VHI`. For 2016 Data, the followings chains are used : `HLT_e26_lhtight_no_ivarloose`, `HLT_e60_lhmedium_nod0`, `HLT_e60_medium` and `HLT_e140_lhloose_nod0`.

The trigger performances can be found here [15] and [16].

5.2.2. Trigger matching and corrections

The `HLT` triggers objects should be matched to the offline objects and the p_{T} of the offline lepton has to be greater or equal to $1.05{\cdot}p_{\mathrm{T}}$ trigger threshold. Thus the lepton p_{T} is required to be above 27 GeV in one or two lepton analysis, except that in one lepton chennel we require the muon p_{T} to be above 25 GeV as we use $E_{\mathrm{T}}^{\mathrm{miss}}$ trigger instead of muon trigger for single muon events. There are also proper trigger SF and systematics derived by CP groups. The SF are defined for the OR of triggers we are using. All these recommendations are coming from [17] for electrons and [18] for muons.

5.2.3. 2-leptons specificities

The single muon trigger SFs combinatoric is already computed for us from the two muons by the muon trigger tool. Concerning the electron we have to compute by ourself the event weight associated to the two electrons trigger SF, as follow :

$$\frac{1-(1-\epsilon^{e1}_{\mathrm{MC}}\times \mathrm{SF}^{\mathrm{e1}})\times(1-\epsilon^{\mathrm{e2}}_{\mathrm{MC}}\times \mathrm{SF}^{\mathrm{e2}})}{1-(1-\epsilon^{e1}_{\mathrm{MC}})\times(1-\epsilon^{e2}_{\mathrm{MC}})} \tag{6}$$

It has been decided to not use di-lepton trigger items in a first time because it has been found that the signal gain acceptance from adding such items in the OR of single lepton trigger is around 2%. Detailed results on these study can be found here [19] for 2015 Data and here [20] for 2016 Data. The study of trigger option for 2 lepton analysis can be found here [21].

For the $e-\mu$ control region, the electron and muon triggers are considered as independant. So we require first the event to pass the single electron trigger OR (and we apply the associated SF). If the event is not firing these items, we check if the event fires the muon trigger OR (and we apply the associated SF).

6. Lepton Selection

$VH(\rightarrow b\bar{b})$, $A \rightarrow Zh(\rightarrow b\bar{b})$, and HVT analyses are categorized by the number of observed leptons (e or μ). The final state of WH channel has one isolated lepton from the leptonic decay of W. The final states of ZH channel have no charged lepton ($Z \rightarrow \nu\nu$) or two leptons ($Z \rightarrow \ell\ell$) depending on the decay of Z boson. The presence of isolated lepton is crucial to reduce fake-lepton background (e.g. QCD multi-jets in 1-lepton channel). A new lepton isolation is introduced to reject the multi-jets background and derive the multi-jet background modeling. In this section the definition of electron and muon selection criteria and optimization studies are described. The systematic uncertainties related to lepton objects are described in Sec 11.

6.1. Electron Reconstruction and Identification

In this subsection a electron reconstruction and an identification algorithm are described. We define VH-loose electron and VH-signal electron criteria. Because of the different background level from fake lepton, 1 lepton and 2 lepton analyses use different lepton selection criterion to maximize sensitivity. Each analysis must be mutually orthogonal by the number of VH-loose electrons and VH-signal electrons.

Electromagnetic (EM) clusters are reconstructed with a sliding window algorithm [22]. EM clusters are associated with a track refitted with GSF [23] to account for bremsstrahlung energy losses. No vertex from conversion is required for the EM cluster of the electron candidate.

Electron identification is performed using likelihood-based method. Variables used by likelihood identification are the longitudinal and transverse shower profiles, track quality, the track and cluster positions to match in η and ϕ and the presence of high-threshold TRT hit. The likelihood-based method allows the inclusion of discriminating variables that are difficult to use with explicit requirement without incurring significant efficiency loss. The detailed performance of likelihood identification can be found in [24, 25].

6.1.1. VH-Loose and VH-Signal Electron Selection

VH-loose electron criteria is defined to allow for the maximum electron selection efficiency for signal processes. Electron p_{T} is required to be greater than 7 GeV. The electron cluster should be in the range of $|\eta| < 2.47$. Loose likelihood identification is applied in VH-loose criteria. Impact parameter significance less than 5 s.d. and $|\Delta z_0 \sin\theta| < 0.5$ mm are also required to reject tracks from pile-up. Track isolation is applied to reduce jet-faking electrons. The isolation selection is chosen to keep 99% efficiency for real electrons [26].

ZH-signal electron criteria requires a electron object with $p_{\mathrm{T}} > 27$ GeV in addition to VH-loose electron criteria for the 1-lepton and 2-lepton channel.

In WH 1-lepton analysis tighter lepton selection is required to suppress multi-jet background. Therefore medium likelihood identification and tighter isolation selection are required (WH-signal). The tight isolation criteria using calorimeter-based isolation keeps 95% signal efficiency [26].

6.2. Muon Reconstruction

In Run-2, ATLAS uses a unified chain for the muon reconstruction [27–29]. There are four muon reconstruction algorithms (Combined, Standalone, SegmentTagged, CaloTagged) using ID track and/or muon spectrometer track and deposited energy in the calorimeter. The muon spectrometer coverage is $|\eta| < 2.7$, while the inner tracker coverage is $|\eta| < 2.5$. A muon standalone algorithm is available for $|\eta| > 2.5$ to find muons in the forward region. All muons with $|\eta| < 2.5$ are required to pass the ID track quality cut recommended by MCP group [18, 30]. Almost all muons pass the combined muon criteria, but there is geometrical efficiency loss due to limited coverage of muon detector. To increase muon acceptance, muon algorithms requiring only muon segment and calorimeter deposit, which is consistent with muon energy loss, are available in $|\eta| < 0.1$ region. Figure 10 shows acceptance coverage on muon η for various muon reconstruction algorithms.

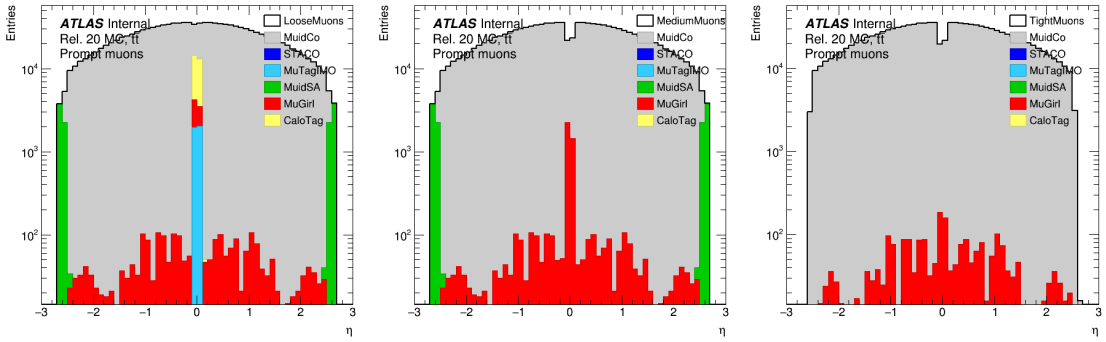

Figure 10: Acceptance coverage for various muon reconstruction algorithms. From left to right, the loose, medium, and tight muon qualities are presented.

6.2.1. VH-Loose and VH-Signal Muon Selection

VH-loose muon criteria is defined to keep muon from signal as much as possible. In VH-loose criteria muon with $p_{\mathrm{T}} > 7$ GeV, impact parameter significance less than 3 s.d. and $|\Delta z_0 \sin\theta| < 0.5$ mm to reject pile-up and cosmic muons are required [31]. Loose muon quality (including Combined, Standalone, SegmentTagged, CaloTagged muons) is required [18]. Track isolation is applied to reduce jet-faking muon. The isolation selection is chosen to keep 99% efficiency for the signal muons [26].

ZH-signal muon criteria requires muon object with $p_{\mathrm{T}} > 27$ GeV and $|\eta| < 2.5$ in addition to the VH-loose muon criteria for the 2-lepton channel.

In WH 1-lepton analysis a tighter lepton selection is required to suppress multi-jet background. For the 1-lepton channel a muon with $p_{\mathrm{T}} > 25$ GeV is required. A tigheter track based isolation criteria is applied with 95% signal efficiency [26].

6.2.2. Muon selection for muons inside jets

It is important to find muons derived from B-hadron semileptonic decays for better b-jet energy resolution, because this contribution is not taken into account in b-jet energy (except for its behaviour as a minimum

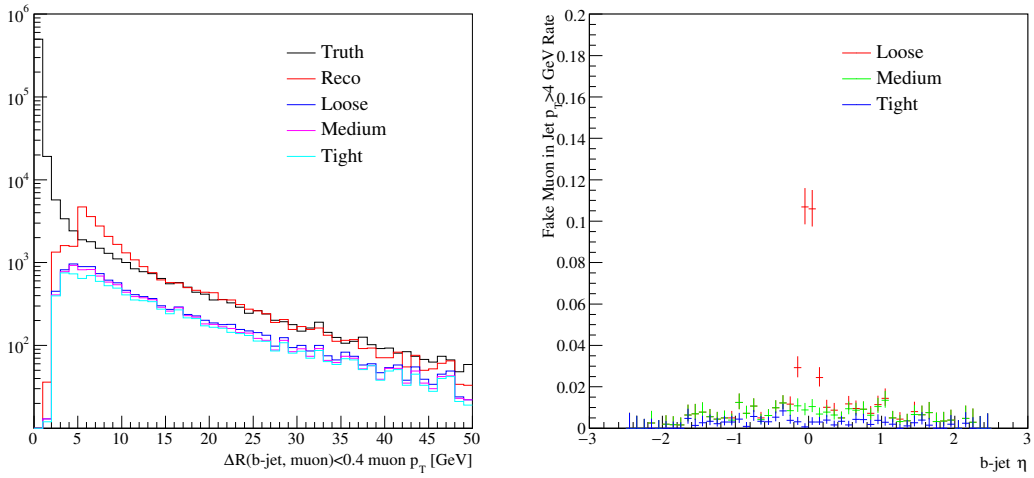

Figure 11: Left: muon p_{T} distribution for various muon quality. muons inside jet are selected by $\Delta R_{b-\mathrm{jet},\mu} < 0.4$. Right: η distribution of fake muon inside jet. Fake muons are selected from jets without Truth muon.

ionising energy in the calorimeter). This is taken into account by the muon-in-jet correction, described in Section 7.3.2. Figure 11 shows the p_{T} distribution of the muons inside jets, defined by $\Delta R(\mu, \mathrm{jet}) < 0.4$, for different reconstruction criteria, as well as the fake rate as a function of jet η in the SM $ZH(\rightarrow b\bar{b})$ signal. Typically muons inside jets have low p_{T} and are not isolated. Therefore the muons inside jets are required to have $p_{\mathrm{T}} > 5$ GeV, $|\eta| < 2.7$ and medium quality (Combined and Standalone), in order to reduce fake muons [18] from CaloTagged and SegmentTagged muon in $|\eta| < 0.1$. If multiple muon candidates are found, one muon which is closest to jet direction in ΔR is chosen and others are not included. The code that does the selection is also seen in the in the Twiki [32].

The muon inside large-R must have $p_{\mathrm{T}} > 10$ GeV, $\eta < 2.5$, use the Combined correction scheme and be within $\Delta R = 0.2$ of one of the two b-tagged track-jets. Such a track jet must have $p_{\mathrm{T}} > 10$ GeV, $\eta < 2.5$, be constituted by at least two tracks, and be ghost-associated to the large-R jet. If more than two muons are matched to the same track jet, only the one closest in ΔR is selected.

Same muon quality is used for both the small-R jet and the large-R jet.

6.2.3. Electron selection for electrons inside jets

It is also important to find electrons derived from B-hadron semileptonic decays for better b-jet energy resolution. Although their contribution is taken into account in the electromagnetic part of the calorimeter-reconstructed jet, the electron neutrino aso produced is not taken into account. This is attempted by the PtReco and Regression corrections described in Section 7.3.2.

The electron-in-jet identification criteria used by the PtReco correction when counting the number of electrons inside the jet are those of an isLooseLH electron with $|\eta| < 2.7$. For this requirement the electron η is used if the electron candidate does not have a calorimeter cluster. If it has one, the variable `etaBE(2)` of the calorimeter cluster is used. The electron is rejected if the variable

Electron Selection	p_T	η	ID	d_0^{sig} w.r.t. BL	$\lvert\Delta z_0 \sin\theta\rvert$	Isolation
VH-Loose	>7 GeV	$\lvert\eta\rvert < 2.47$	LH Loose	< 5	< 0.5 mm	LooseTrackOnly
ZH-Signal	>27 GeV			Same as VH-Loose		
WH-Signal	Same as VH-Signal		LH Tight	Same as VH-Signal		FixedCutHighPtCaloOnly

Table 7: Electron Selection

Muon Selection	p_T	η	ID	d_0^{sig} w.r.t. BL	$\lvert\Delta z_0 \sin\theta\rvert$	Isolation
VH-Loose	>7 GeV	$\lvert\eta\rvert < 2.7$	Loose quality	< 3	< 0.5 mm	LooseTrackOnly
ZH-Signal	>27 GeV	$\lvert\eta\rvert < 2.5$		Same as VH-Loose		
WH-Signal	>25 GeV	$\lvert\eta\rvert < 2.5$	Medium quality	< 3	< 0.5 mm	FixedCutHighPtTrackOnly

Table 8: Muon Selection

`isGoodOQ(xAOD::EgammaParameters::BADCLUSELECTRON)` is false. The electron candidate is also required to have $p_T > 5$ GeV. The code that does the selection is also seen in the in the Twiki [32].

6.3. Tau Veto

In 0 lepton channel, $t\bar{t}$ and W/Z+jets including τ are large contributions. It is efficient way to reduce background events including τ lepton by vetoing τ object. Hadronic decay of τ leptons (τ_{had}) are characterized by having one or three charged particles (prongs) with a neutrino and neutral pions. The reconstruction of visible τ decay starts with jets anti-k_t algorithm with a size parameter value $\Delta R = 0.4$ [33]. The $\tau_{had-vis}$ p_T is set to the total energy of TopoClusters within $\Delta R < 0.2$. Tracks associated to the $\tau_{had-vis}$ are required to be in the core region $\Delta R < 0.2$ around the τ direction. Tau candidates are required the following selections:

- $p_T > 20$ GeV
- $|\eta| < 2.5$ excluding crack region, $(1.37 < |\eta| < 1.52)$
- 1 or 3 tracks

BDT based tau identification is used to reject the background from jet. In the 0 lepton channel, events having any tau objects of medium quality [34, 35] are rejected. The background (mainly $t\bar{t}$) can be rejected by 6-9% in three and more than three jets events, while $A \to Zh$ signal loss can be kept less than 1%. In SM analysis tau veto causes significant signal loss due to $WH \to \tau\nu b\bar{b}$ contribution. It is not applied in the SM analysis.

6.4. Final Lepton Selection

The final lepton selection in $VH(\to b\bar{b})$ analysis is summarized. Table 7 (8) presents a summary of electron (muon) selection criteria, for VH-loose, ZH-signal and WH-signal, respectively.

7. Jets

Most quarks manifest themselves in the detector as a directional spray of tracks and calorimeter deposits known as jets. This is true of the b-quark initiated jets (b-jets) produced by the Higgs boson in our signal processes. Jets initiated from other quarks or gluons as well as b-quarks are present in all of our background processes as well. Thus, jets play an important role in identifying event topologies and kinematics consistent with our signal processes. bQuarkSemileptonicDecay

7.1. Jet Collections

7.1.1. Standard-R jet collections

The primary jet collection used in our analysis is reconstructed from topological calorimeter-cell clusters calibrated using the EM calorimeter scale [36]. These clusters are then used as input to the anti-k_t algorithm [37] with a radius parameter of R=0.4 to reconstruct jet objects. The name of the collection is `AntiKt4EMTopoJets` in the xAODs used in this analysis.

In order to suppress jets arising from pileup a new likelihood-based discriminant is used for Run-2 called the Jet Vertex Tagger (JVT [38]). JVT uses information about the primary vertex, jet p_{T}, and track p_{T} to construct a 2-D likelihood that is robust against potential jet flavor and training sample biases. It is trained on jets within a kinematic range that is expected to be sensitive to pileup (20 GeV < p_{T} < 60 GeV and $|\eta| < 2.4$) and calibrated with $Z \rightarrow \mu\mu$ + jets samples. Thus, JVT is only used on jets within this kinematic range. JVT is calculated on uncalibrated jets during reconstruction. Therefore, the JVT must be recalculated with the `JetVertexTaggerTool`. The JetEtMiss provides a tool for computing a JVT-based pass/fail decision given an `xAOD::Jet`. This tool (called `JetJvtEfficiency`) also provides efficiency scale factors at various efficiency working points. The list of available working points are given in Table 9. We use the "`Default`" (also known as "`Medium`" in the tool) working point for our `AntiKt4EMTopoJets`.

Working Point	JVT Cut	Average efficiency [%]
Loose	0.11	97
Default	0.59	92
Tight	0.91	85

Table 9: JVT working points available.

Jets are classified as either "signal" or "forward". Signal jets are eligible for b-tagging and used in reconstructing the Higgs boson. As such, the requirements placed on signal jets are consistent with the flavor tagging CP group's recommendation for b-jet tagging. The full set of selection requirements is given in Table 10.

7.1.2. Large-R jet collections

For signal processes with a large resonant mass the b-jets produced by the Higgs may be too close together to be resolved by the R=0.4 calorimeter-based jets (calo-jets). This effect is expected to be noticeable

Jet Category	Selection Requirements
Forward Jets	jet cleaning $p_{\mathrm{T}} > 30\,\mathrm{GeV}$ $2.5 \leq \lvert\eta\rvert < 4.5$
Signal Jets	jet cleaning $p_{\mathrm{T}} \geq 60\,\mathrm{GeV}$ $\lvert\eta\rvert < 2.5$ or $20\,\mathrm{GeV} \leq p_{\mathrm{T}} < 60\,\mathrm{GeV}$ $\lvert\eta\rvert < 2.4$ JVT > 0.59

Table 10: `AntiKt4EMTopoJets` selection requirements. Jet cleaning refers to the quality criteria interfaced through the JetCleaningTool CP tool. This tool removes jets in regions with hot noisy calorimeter cells.

when $p_{\mathrm{T}}^{\mathrm{H}} \gtrsim 600\mathrm{GeV}$[1]. Our approach to resolving the signal b-jets in this "merged" regime is to use a large-R jet with large invariant mass and search for smaller-R track-based jets (track-jets) ghost-associated to this large-R jet that pass our b-tagging requirements. Specifically, we define a large-R jet with R=1.0 and smaller track-jet with R=0.2. In order to minimize the effects from pileup, R=0.2 calo-jets with less than 5% of the large-R jet p_{T} are removed from consideration. b-tagging is then applied to the ghost-associated, R=0.2 track-jets. The name of the large-R jet and track-jet containers used in this analysis are `AntiKt10LCTopoTrimmedPtFrac5SmallR20Jets` and `AntiKt2PV0TrackJets`, respectively. The full set of selection requirements is given in Table 11.

Jet Category	Selection Requirements
Large-R Jets	$p_{\mathrm{T}} > 200\,\mathrm{GeV}$ $\lvert\eta\rvert < 2.0$
Track-Jets	$p_{\mathrm{T}} > 10\,\mathrm{GeV}$ $\lvert\eta\rvert < 2.5$ has at least 2 track constituents

Table 11: AntiKt10LCTopoTrimmedPtFrac5SmallR20Jets (large-R jet) and AntiKt2PV0TrackJets (track-jet) selection requirements.

7.2. b-tagging

The jets from the Higgs boson in our signal process should originate from b-quarks. It is, therefore, desirable to be able to distinguish b-jets from light-, τ-, and c-jets.

7.2.1. Truth-level flavor labelling

Truth-level flavor labelling for both calo jets and track jets is accomplished through the following procedure, using a maximum cone reconstructed parameter $R_{\mathrm{max}} = 0.3$:

[1] Using the rule of thumb $\Delta R = 2m/p_{\mathrm{T}}$, where $m = m_{\mathrm{H}}$ and $\Delta R = 0.4$

1. If a weakly decaying b-hadron is found within $\Delta R < R_{\text{max}}$ of the jet direction, the jet is labeled a b-jet.
2. If a b-hadron isn't found, then if a weakly decaying c-hadron is found within $\Delta R < R_{\text{max}}$ of the jet direction, the jet is labeled a c-jet.
3. Otherwise, if a τ-lepton is found within $\Delta R < R_{\text{max}}$ of the jet direction, the jet is labeled a τ-jet.
4. If any hadron/τ-lepton matches more than one jet, the closest jet is chosen.
5. All unlabeled jets after steps 1 through 4 are labeled light-jets.

7.2.2. Direct tagging

The standard algorithm for b-jet tagging in Run-2 after the Athena release 2.7 is the MV2c10 discriminant. This algorithm uses log-likelihood ratios from IP2D and IP3D[2], secondary vertex information from SV1, information about the relationship between the primary and secondary vertices from JetFitter, and the p_{T} and η of the jet [39]. This information is used as input to a boosted decision tree to produce the final discriminant. The algorithn is trained on 5 million $t\bar{t}$ events with a mixture of (1-xx)% light-jet and 10% c-jets as background. This additional c-jet contamination gives better c-jet rejection with minimal degradation of light-jet rejection.

The flavor tagging CP group provides two tools for using b-tagging information. The first tool, `BTaggingEfficiencyTool`, provides tagging efficiencies for MC jets and MC-to-Data scale factors (SF). Both the efficiencies and SF depend on the jet's p_{T} and η. The second tool (`BTaggingSelectionTool`) provides a unified interface to determine whether a jet is b-tagged or not. It takes jet kinematics and JVT requirements into account. The standard interpretation for an MV2c10 working point is that the light-jet and c-jet rejections are roughly constant over the kinematic range of the jet, while the efficiency is allowed to vary over a certain kinematic range of the jet. The `BTaggingSelectionTool` has the capability to hold the b-tagging efficiency constant, while varying the light- and c-jet rejection rates. The available b-tagging efficiencies for the algorithm MV2c10 is shown in Table 12.

name	MV2c10 weight cut	b-tagging efficiency [%]	c RR	light RR
AntiKt4EMTopoJets				
FixedCutBEff_60	0.9349	60.03	34.54	1538.78
FixedCutBEff_70	0.8244	69.97	12.17	381.32
FixedCutBEff_77	0.6459	76.97	6.21	134.34
FixedCutBEff_85	0.1758	84.95	3.10	33.53

Table 12: b-tagging working points available for MV2c10. RR is the rejection rate (the inverse of efficiency).

7.2.3. Truth tagging

Removing events which do not pass a given b-tagging criteria can create issues with low statistics during multivariate analysis (MVA) training/testing and the template fitting process. One way to overcome this

[2] IP2D uses transverse impact parameter information, while IP3D additionally uses the longitudinal impact parameter.

issue is not to cut away events due to b-tagging, but apply a weight to each MC event based on the desired number of b-jets, tagging efficiencies, and scale factors. This is broadly referred to as truth tagging because of the use of the truth flavor label of the jet in determining the event weight. Specifically, we select a pair of jets for this truth tagging based on their probablity to be tagged. A detailed description of this method follows.

The three primary components to compute for truth tagging are the event weight (w_{TT}), which jets to "tag," and what tag weight to assign these truth-tagged jets. Given a set of n jets J the set of all m-combinations of jets is denoted $\binom{J}{m}$, the i^{th} combination $\binom{J}{m}_i$, and $\overline{\binom{J}{m}}_i = J - \binom{J}{m}_i$. The efficiency and inefficiency products are

$$\mathcal{E}(J, x) = \prod_{j \in J} \epsilon_x(j)$$

and

$$\mathcal{E}_{\mathrm{in}}(J, x) = \prod_{j \in J} (1 - \epsilon_x(j)),$$

where $\epsilon_x(j)$ is the tagging efficiency for jet j at efficiency working point x. Thus, the event weight for m truth-tagged jets can be expressed as

$$w_{\mathrm{TT}}(x) = \sum_{i}^{\left|\binom{J}{m}\right|} P_i(x),$$

where

$$P_i(x) = \mathcal{E}\left(\binom{J}{m}_i, x\right) \mathcal{E}_{\mathrm{in}}\left(\overline{\binom{J}{m}}_i, x\right).$$

The i^{th} combination is given a probability of being truth-tagged equal to $P_i(x)/w_{\mathrm{TT}}(x)$. A combination is randomly selected to be tagged based on these probabilities. Once tagged, the jets are assigned tagweight values through the following steps. Given the set of efficiency working points (WPs) X and a selected WP $\mathbf{x}$ the set of WPs equal to or less $\mathbf{x}$ is terms of efficiency is denoted $X_{\leq \mathbf{x}}$. For truth-tagged jet j the probability to associate this jet with a specific WP x ($x \leq \mathbf{x}$) is

$$P_{\mathbf{x}}(j, x) = \frac{\epsilon_x(j)}{\sum_{i \in X_{\leq \mathbf{x}}} \epsilon_i(j)}$$

A specific WP is randomly selected for jet j from $X_{\leq \mathbf{x}}$ using the probabilities computed from by $P_{\mathbf{x}}(j, x)$. Finally, a tagweight tw_{TT} is computed for a randomly selected WP with tagweight tw_{sel} by

$$tw_{\mathrm{TT}} = \frac{1}{2}\left(tw_{\mathrm{sel}} + tw_{\mathrm{sel}-1}\right)$$

where $tw_{\mathrm{sel}-1}$ is the next-lowest tagweight from the selected one. For jets not tagged the procedure for computing the tagweight is the same, except the next-highest WP is chosen rather than the next-lowest.

7.2.4. Flavour tagging scale factors

The scale factors described in this section apply both to the direct and truth b-tagging. The latest CDI file `2016-20_7-13TeV-MC15-CDI-2017-06-07_v2.root` [40] is used. The default calibrations are used: the $t\bar{t}$ PDF method for b-jets and the negative tag method for light jets. For the c-jet, the *a priori* default

$W + c$ calibration method is used includes a large systematic uncertainty due to tension with the $t\bar{t} + c$ method, as illustrated in Figure 12. Instead, we are using the $t\bar{t} + c$ method as default, as this has reduced c-jet scale factor (SF) uncertainties, as well as resulting in nuisance parameters (NP) which are pulled less in the conditional fit to data.

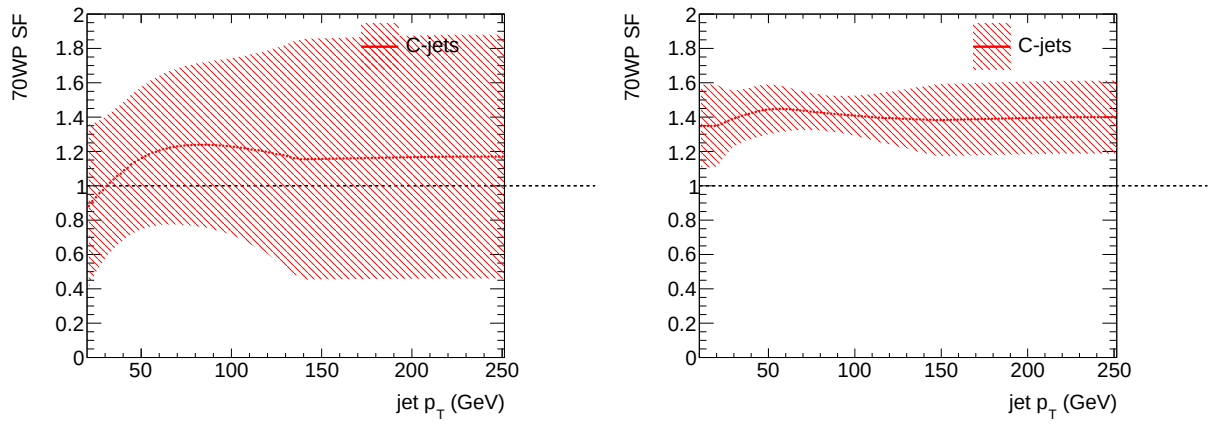

Figure 12: Comparison of the c-jet scale factors and their corresponding uncertainties from the $W + c$ (left) and $t\bar{t} + c$ (right) calibrations.

7.3. Normal-R-jet energy corrections

Jets from both MC and data need energy corrections applied to improve their 4-vector reconstruction given event topologies. Jets from MC need in addition to have their modelling in agreement with data. Jet energy resolution (JER) in MC must be smeared to more accurately reflect actual detector conditions. The JetEtMiss CP group provides corrections that are applied to all jets. Special corrections dedicated to b-jets are then applied.

7.3.1. Flavor-inclusive corrections

For Run-2 the `JERSmearingTool` CP tool is provided to smear MC jets and evaluate the JER systematic uncertainty. Jets reconstructed in data are calibrated with the `JetCalibrationTool` CP tool. This corrects for the origin, η, jet energy scale (JES) [41], as well as performing a global sequential calibration (GSC) [42]. GSC uses the percentage of the total energy deposited in the last layer of the electromagnetic calorimeter, in the first layer of the hadronic calorimeter, the jet width calculated with tracks, and the number of tracks to improve the JER and the difference in response between different jet flavors.

The jet energy calibrations offered by the JetEtMiss CP group are derived to improve a collection of jets where the light-jets carry the most weight. They are then applied uniformly to all jets, irrespective of their origin. Since jets of different flavors have different behaviour of the GSC input variables, the same GSC correction affects the jets differently depending on their origin. As a result, the jet energy response agrees more between different jet flavors. Since our signal contains two b-jets originating from a resonance and the di-b-jet invariant mass ($m_{b\bar{b}}$) is a good signal to background discriminant, further specific b-jet energy corrections are needed to account for b-jet and resonant specific effects.

7.3.2. *b*-jet-specific corrections

The *b*-jet specific corrections are applied after the event selection is fixed. Jet counting is based on jets at the GSC (Nominal) scale. The *b*-jet energy corrections improve *b*-jet p_{T}'s both scale and resolution. The final discrimants like $m_{b\bar{b}}$, and the BDT output (which uses as inputs $m_{b\bar{b}}$, but also other quantities dependent of jet p_{T}), have an improved scale and resolution as a result.

There are several corrections that have been studied. The chosen approach is that of two consecutive corrections. The first correction is the muon-in-jet, while the second is the PtReco correction for the 0- and 1-lepton channels, or the kinematic likelihood (KL) fit for the 2-lepton channel. After an introduction to *b*-jet energy corrections below, the corrections derived *per-jet*, muon-in-jet and PtReco, are described in the following subsections. The correction derived *per-event*, the KL fitter, is described in the Appendix D of the main analysis support note of the VH(bb) search [43].

Muons, muon neutrino, and electron neutrino resulting from *B*-hadron semileptonic decays are not properly accounted for in the jet 4-vector reconstructed in the calorimeter. Even if there is a fully hadronic decay, a non-closure effect appears in the low-p_{T} bins of the jet energy response from decay products depositing their energy in the calorimeter beyond the cone radius of the jet reconstruction algorithm, due to the large impact parameter of the *b*-jet, denoted out-of-cone energy deposition effect. It is called a non-closure effect, as a full closure would mean the response would be very close to one after the JES calibration. However, at low p_{T} the response has large deviations from one. The GSC calibration is designed to improve the resolution while keeping the same response as for JES. The JES was designed to improve the response of a sample of generic jets dominated by light jets. As *b*-jets are special, the jet response is not one, especially at low p_{T}. Another effect is altered kinematic distributions of the p_{T} of the two *b*-jets due to their resonant particle origins.

Two approaches are employed in correcting for these effects. One is to decouple the various effects and has been used by ATLAS in Run-1 VH search [44]. ATLAS also investigates it in Run-2 by proposing two corrections denoted muon-in-jet and PtReco. For the 2-lepton channel, the *per-jet*-derived PtReco is replaced by the *per-event* correction kinematic likelihood fit. The other is to have one correction based on multivariate-based regression. It has been pioneered by CDF [45] in the WH search [46], used by CMS in the VH [47] and VBF [48] searches, and investigated also by ATLAS in the Run-1 [49, 50]. ATLAS has also investigated it in the Run-2. Given a similar performance, the decoupled corrections are prefered.

Examples of code and description about all these corrections studied in Run-2 are documented in the Twiki [32]. The derivation and validation of the consecutive corrections of decoupled approach, muon-in-jet and PtReco, as well as the Regression correction are described in detail in the Jet section and several appendices of the object note of the Hbb group for Moriond 2016 [51]. The two approaches obtain similar performance. The regression is slightly more complex and some of the input jet variables appear to not be well modelled in data. The simpler approach of the decoupled corrections (muon-in-jet followed by PtReco or KL) was chosen for the Moriond 2016 and ICHEP 2016 analyses, while the Regression approach is recognized to have a potential for use in the future.

These corrections are applied for the 2-*b*-tag category to the two *b*-tagged jets, and not to the other non-*b*-tagged jets. $m_{b\bar{b}}$ is computed using both corrected *b*-tagged jets. For the 1-*b*-tag category, the correction is applied only to the single *b*-tagged jet. $m_{b\bar{b}}$ is computed using this corrected *b*-tagged jet and the leading non-*b*-tagged jet that is at the Nominal (GS) calibration coming from the standard JetEtMiss calibration.

7.3.3. *b*-quark semileptonic decays

The *b*-quark inside the *B*-hadron, one of the particles of the *b*-jet, decays to a *c* quark and a *W* boson, while the *c* quark also decays to a *d* quark and another *W* boson. When at either of *W* boson can decay leptonically, while the other decays hadronically, we denote a semileptonic decay of the *b*-jet, as illustrated in the two cases of Figure 13.

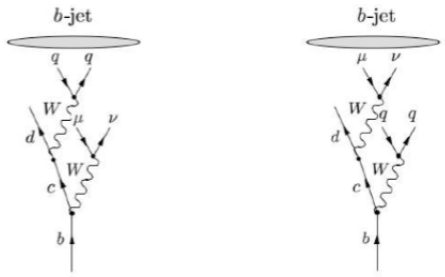

Figure 13: Feynman diagrams of *b*-quark decays, where one of the *W* bosons decays semileptonically to a muon and a neutrino, while the other *W* boson decays hadronically. Either one or the other happen in about 10.6% of the time. The imagine is taken from [52].

A *W* boson decay involving a muon happens in $(10.6 \pm 0.2)\%$ of the cases [53]. In other $(10.7 \pm 0.2)\%$ and $(11.4 \pm 0.2)\%$ of cases, the muon can be replaced by an electron or τ lepton, respectively [53]. The principle of lepton universality predicts that these three numbers are all equal, which they are within the error bands, though at more than one standard deviation. The electron lives forever and the muon decays only outside the detector. However, the τ lepton decays inside the detector. In $(17.41 \pm 0.04)\%$ and $(17.83 \pm 0.04)\%$ of the cases it decays to a muon or electron respectively, plus two neutrinos [53]. These numbers are also predicted by lepton universality to be equal, which they are within the error bands. In other $(0.0036 \pm 0.0004)\%$ and $(1.75 \pm 0.18)\%$ of the cases, the τ lepton decays to a muon or electron, respectively, plus two neutrinos and a photon [53]. In the remaining 63% of the cases, the τ lepton decays to hadrons plus a τ neutrino [53]. Considering these, we conclude that a *W* boson decay is semileptonic to a muon in about 12.6%, semileptonic to an electron about 12.7%, while decaying hadronically in about 74.7% of cases.

There are two *W* bosons in the *b*-quark decay. There are the following probability of the *b*-quark decay: *ee* (1.6%), $\mu\mu$ (1.6%), $e\mu$ (3.2%), *e* had (18.8%), μ had (18.8%), and had had (56.0%). There is at least a muon in at least 44% of cases, as confirmed also in [52].

Not all of these electrons or muons are reconstructed inside the jet, since they have to pass track isolation criteria, overall $\Delta R < 0.4$ of the jet axis and $p_{\mathrm{T}} > 5$ GeV, as described in Sections 6.2.2 and 6.2.3. In practice, about 12% of *b*-tagged jets have a reconstructed muon inside and about 1-2% of them have a reconstructed electron inside. Together we call these *semileptonic jets*, while those with no recostructed electron or muon as *hadronic jets*. This counting is relevant for the PtReco correction, derived separately for these two categories of jets.

7.3.4. Muon-in-jet correction

These muons and electrons are typically removed by the overlap removal procedure. But they do influence the measurement of the jet energy. The electron deposits energy in the calorimeter and its energy is

accounted for in the jet. The muon is a minimum ionising particle, depositing very little energy in the calorimeter. To correct for it, the muon 4-vector is added to the jet 4-vector, while the 4-vector of the energy deposited by the muon in the calorimeter is removed. If there are more than one muon inside the jet (which is possible in 1.6% of cases at truth level) we chose the closest one in ΔR to the jet and correct only for that one. After muon-jet correction, the jet 4-vector is called OneMu.

Systematic uncertainties related to the muon selection for the muon-in-jet correction have been studied in Run-1 and found to be negligible.

7.3.5. PtReco correction

The training target is represented by the particle-level jet TruthWZ, which contains a reconstructed jet with the same algorithm as for the reconstructed jet, using all stable particle of type hadron, and non-isolated neutrinos and muons.

The OneMu 4-vector is then scaled by a correction factor that depends on wether the B-hadron has decayed semileptonically or hadronically, and on the jet p_{T} value. This correction is called PtReco. After the PtReco correction, the jet 4-vector is denoted PtReco. If at least a muon (defined in Section 6.2.2) or an electron (defined in Section 6.2.3) is reconstructed inside the jet (within $\Delta R = 0.4$ around the jet axis), the semileptonic decay is considered for the jet. Otherwise, a hadronic decay is considered. The former case happens in about 13% of jets.

For either case, the PtReco correction is derived in bins of p_{T} of the reconstructed jet at the OneMu stage, up to 300 GeV. The bin edges are optimised so that they contain approximately the same number of events. A PtReco histogram of the correction factors is built by setting for each jet p_{T} bin the content of the value of the mean of the distribution of the ratio of the p_{T} of the TruthWZ jet to the OneMu jet is filled to a histogram. To allow for a smooth distribution, the histogram is interpolated using the `TH1::Interpolate(pt)` method. As illustrated in Figure 14, the main feature of the PtReco correction factors is that for hadronic jets they increase the jet 4-vector with around 12% at low p_{T} and decreases at high p_{T} to a plateau at around 1%, while for semileptonic jets the correction factors are about 10% larger across the jet p_{T} spectrum to account also for the neutrino from the semileptonic decays. The interpolation is show to be stable also for jets with p_{T} larger than 300 GeV.

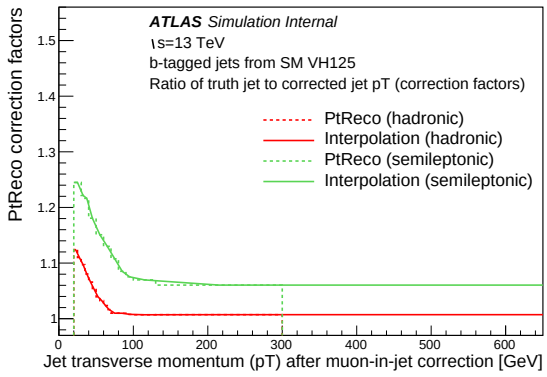

Figure 14: PtReco histogram wit both bin content and interpolation, for both semileptonic and hadronic jets, trained in SM VH with $H \to b\bar{b}$.

7.3.6. Correction comparison

To compare the different reconstructed jet p_{T} scale with the target TruthWZ, events are selected with exactly two good quality jets with $p_{\mathrm{T}} > 20$ GeV, b-tagged and having a TruthWZ particle-level-jet matched to them in $\Delta R < 0.4$. Events are split based on weather their two jets decay or not semileptonically or hadronically. The $m_{b\bar{b}}$ plots are shown in Figure 15. Each of the consecutive corrections (muon-in-jet and PtReco) improves both the width, peak and resolution (width divided by peak). The impact of the corrections increases with the number of jets that decay semileptonically.

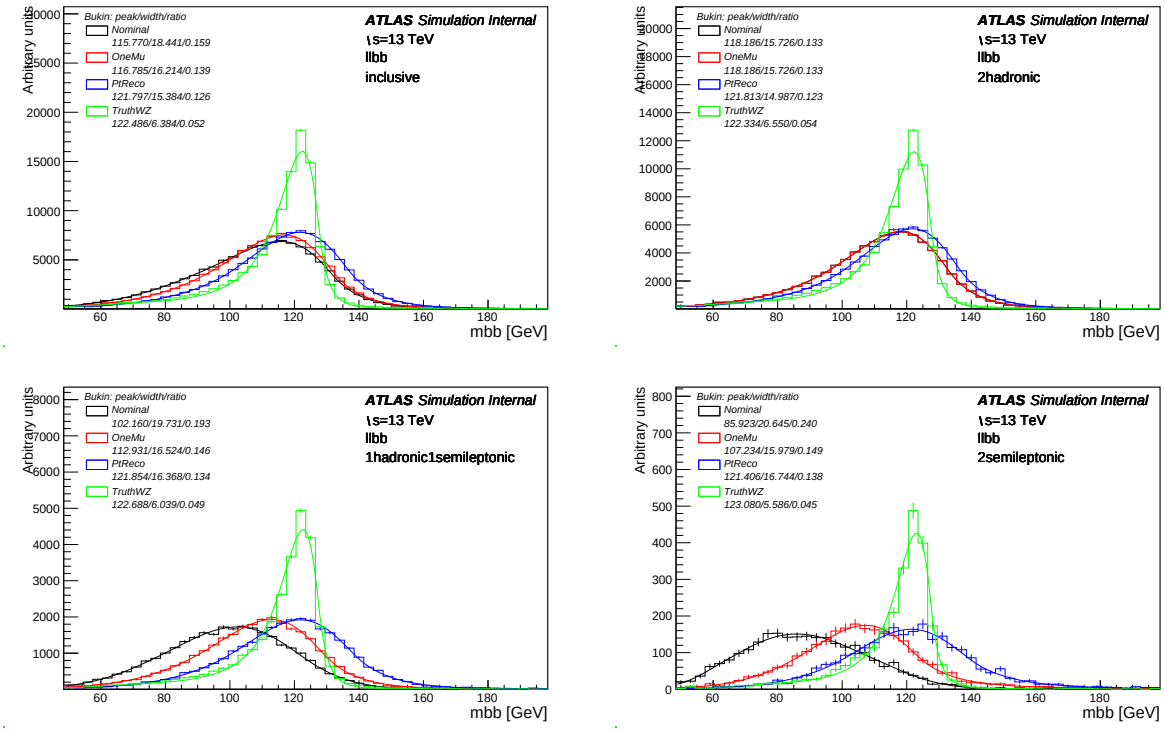

Figure 15: Comparison of $m_{b\bar{b}}$ for the Nominal (GSC), muon-in-jet, PtReco and the target of TruthWZ, for the following event categories: inclusive (top left), 2 hadronic (top right, about 79% of events), 1 hadronic and 1 semileptonic (bottom left, about 20% of events) and 2 semileptonic (bottom right, about 1% of events). Distributions are fit with a Bukin function and the fit parameters are shown in the legend.

7.3.7. Correction validation in $Z + b$ data vs MC

The muon-in-jet + PtReco corrections have been studied in the $Z + b$ sample [54].

In both data and MC both b-jet scale and resolution are improved over the GSC corrections, as illustrated in Figure 16. They exhibit a similar performance to the more complex MVA-based regression. This confirms the choice of the decoupled muon-in-jet + PtReco approach.

Data and MC show good agreement to each other, as seen in Figure 17. As such, no extra systematic is assigned to the PtReco correction. When jets are systematically varied by their JES or JER jet systematic, the muon-in-jet and PtReco corrections are applied on the top of those.

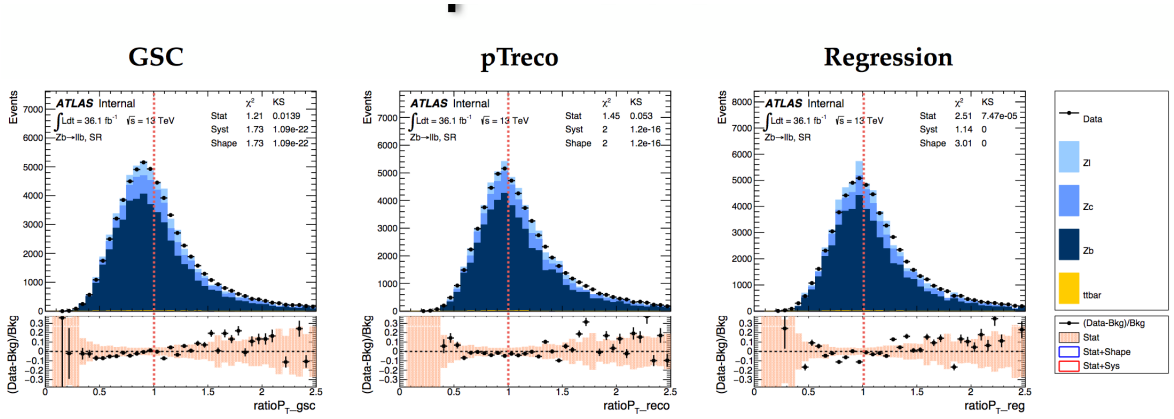

Figure 16: The ratio between the jet p_{T} and Z boson p_{T}, for the inclusive jet sample, for GSC, muon-in-jet + PtReco and MVA-based regression.

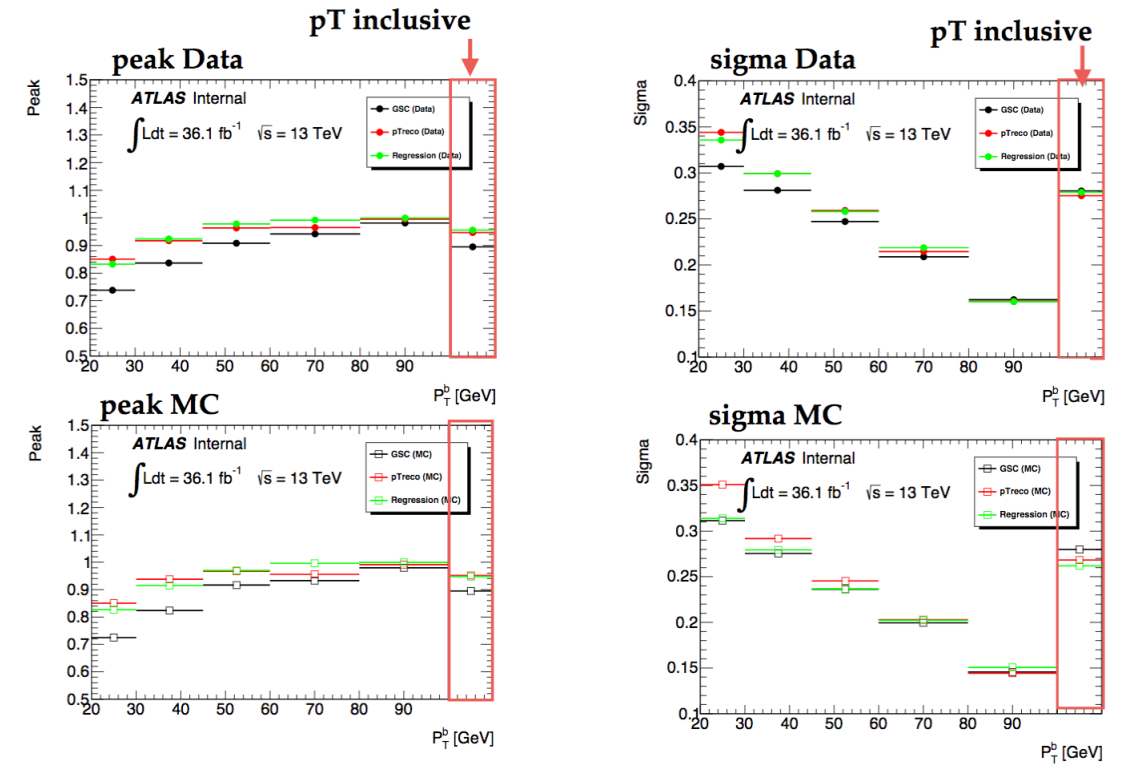

value in inclusive	GSC	pTreco	Regression
peak (Data/MC)	0.895/0.895	0.947/0.952	0.956/0.947
sigma (Data/MC)	0.280/0.280	0.275/0.268	0.279/0.262

Figure 17: For different bins of jet p_{T}, there are illustrated peak and sigma (or width of the core) of fits to Bukin functions of the ratio between the jet p_{T} and Z boson p_{T}, as a measure of scale and resolution, respectively. Comparing data (top) and MC (bottom). Overlaying GSC, muon-in-jet + PtReco and MVA-based regression.

7.4. Large-*R*-jet energy corrections

b-jet energy corrections are needed also for large-*R* jets used in the merged regime. Since the SM VH(bb) does not use a merged regime, the large-*R* jets combined mass through the Xbb tagger [55].

In both the Run-1 analyses and the present Run-2 analysis, only the muon-in-jet correction is applied. A quick study of PtReco derivation using TruthWZ, which is also trimmed, just as the reconstructed jet, as a target [56], suggests that there is no significant gain in large-*R* jet mass reconstruction if a PtReco is applied to the large-*R* jet. *A priori* the PtReco should have an smaller impact for the large-*R*-jet mass. The mass increases by the same factor as the jet p_{T}. However, for the resolved regime, two different factors of change for the two jet p_{T} can lead to a different change in the mass of the Higgs candidate. The muon-in-jet selection for Moriond 2016 is applied using the Xbb tagger. For ICHEP 2016, it was used the SM VH(bb) muon-in-jet style again. For summer of 2017, there is an improved Xbb with combined mass.

8. Overlap Removal Procedure

During LS1 there was an effort to harmonize the treatment of the overlap removal (OR) between different analysis groups. A recommendation has been defined in [57] and an updated version has been defined for Moriond 2016 analysis [58]. This harmonization procedure is the baseline method used in Hbb. The official ASG tool [59] is used for the overlap removal, with only one difference: no b-tagging information is used in the jet-muon OR, as the jet is not considered for OR if it is b-tagged. It has been found that the effect of not applying this overlap has small impact.

Only preselected objects with `Props::passPreSel = true` among electrons, muons, small-R jets, large-R jets and τ leptons are considered. The individual overlap removals are done in the following sequence of steps, where objects are considered at a given step only if they were not removed at the previous step:

- **tau-electron:** If $\Delta R(\tau, e) < 0.2$, the τ lepton is removed.
- **tau-muon:** If $\Delta R(\tau, \mu) < 0.2$, the τ lepton is removed, with the exception that if the τ lepton has $p_{\mathrm{T}} > 50$ GeV and the muon is not a combined muon, then the τ lepton is not removed.
- **electron-muon:** If a combined muon shares an ID track with an electron, the electron is removed. If a calo-tagged muon shares an ID track with an electron, the muon is removed.
- **electron-jet:** If $\Delta R(\mathrm{jet, e}) < 0.2$ the jet is removed. For any surviving jets, if $\Delta R(\mathrm{jet}, e) < \min(0.4, 0.04 + 10\ \mathrm{GeV}/p_{\mathrm{T}}^{e})$, the electron is removed.
- **muon-jet** If $\Delta R(\mathrm{jet}, \mu) < 0.2$ or the muon ID track is ghost associated to the jet, then the jet is removed if the jet has less than three associated tracks with $p_{\mathrm{T}} > 500$ MeV ($\mathrm{NumTrkPt500PV}^{\mathrm{jet}} < 3$) or both of the following conditions are met: the p_{T} ratio of the muon and jet is larger than 0.5 ($p_{\mathrm{T}}^{\mu}/p_{\mathrm{T}}^{\mathrm{jet}} > 0.5$) and the ratio of the muon p_{T} to the sum of p_{T} of tracks with $p_{\mathrm{T}} > 500$ MeV associated to the jet is larger than 0.7 ($p_{\mathrm{T}}^{\mathrm{muon}}/\mathrm{SumPtTrkPt500PV}^{\mathrm{jet}} > 0.7$).
  For any surviving jets, if $\Delta R(\mathrm{jet}, \mu) < \min(0.4, 0.04 + 10\ \mathrm{GeV}/\mathrm{p}_{\mathrm{T}}^{\mu})$, the muon is removed.
- **tau-jet:** If $\Delta R(\tau, \mathrm{jet}) < 0.2$, the jet is removed.
- **electron-fat jet:** If $\Delta R(e, \mathrm{fat\ jet}) < 1.2$, the fat jet is removed.

9. Missing Transverse Momentum

The missing transverse momentum (MET, or $E_{\mathrm{T}}^{\mathrm{miss}}$) plays a key role in two of our signal channels: 0- and 1-lepton. These channels contain a vector boson that decays either to two neutrinos or one lepton plus a neutrino. In either case the neutrino is not directly detectable and, thus, appears only as an imbalance in transverse momentum[3]. In the 2-lepton channel the amount of MET is limited to suppress background. MET is comprised of the negative vector sum of p_{T} of physics objects (leptons, jets, etc.) and a so-called soft term. MET in Run-2 is reconstructed using a track-based soft term (TST) [60] in addition to the hard terms arising from photons, electrons, muons, τ leptons, and jets. The TST is made of good-quality tracks not associated with the hard term. Since these quality tracks are associated with the primary vertex, the TST term is robust against pile-up. Missing transverse momentum can also be constructed based on inner detector tracks ($E_{\mathrm{T,trk}}^{\mathrm{miss}}$). This provided a robust estimate of the MET while being less sensitive to effects from pileup. However, since $E_{\mathrm{T,trk}}^{\mathrm{miss}}$ is based mostly on tracks left by charged particles it cannot account for neutral particles. MET is rebuilt using a tool provided by the JetEtMiss CP group called the `METMaker` [61], which requires the hard object containers used in the analysis. This tool also allows an analysis to select between using the calorimeter-based jets (`rebuildJetMET`) or track-based jets (`rebuildTrackMET`). The containers we use for calorimeter-based and track-based MET are `MET_Reference_AntiKt4EMTopo` and `MET_Track`, respectively.

An additional variable called METHT, defined in Equation (7),

$$\mathrm{METHT} = \frac{E_{\mathrm{T}}^{\mathrm{miss}}}{\sqrt{\sum p_{\mathrm{T}}^{e} + \sum p_{\mathrm{T}}^{\mu} + \sum p_{\mathrm{T}}^{\mathrm{jet}}}}\,, \tag{7}$$

can be used in event selection. It is defined as the MET divided by the (scalar) p_{T} sum-in-quadrature of the hard objects in the event. Since the denominator in Equation (7) is proportional to the MET resolution, cutting on METHT is equivalent to making harder cuts on better-resolved MET and looser cuts on worse-resolved MET.

[3] Transverse momentum is defined as the components of momentum in the plane perpendicular to the beam axis.

10. Event Preselection

10.1. DxAOD

The derivation cuts are summarized in Tables 1, 2, and 3.

10.2. CxAOD

The CxAOD cuts are summarized in Table 13 and described below:

- **lepton selection** no VH-loose lepton (0-lepton analysis), 1 tight + 0 VH-loose (1-lepton analysis) and 2 VH-loose (2-leptons analysis),
- **pass GRL** for data only, events passing the GRL,
- **has PV** events having a primary vertex,
- **is clean event** for data only, no Tile, LAr, SCT and Core error,
- **bad jet cleaning** discard event if it has any bad jets with $p_{\mathrm{T}} > 50$ GeV or $20 > p_{\mathrm{T}} > 50$ GeV and $|\eta| < 2.4$ and JVT > 0.64,
- **jets pre-selection** at least one signal jet or at least one large-R jet.

Then, optimized selection is determined for every analysis channels. This final selection is described in analysis notes.

0 lepton	1 lepton	2 leptons
lepton veto	exactly 1 lepton	exactly 2 leptons
	data: pass GRL	
	has PV	
	data: is clean event	
	bad jet cleaning	
	jets pre-selection	

Table 13: CxAOD selection.

11. Experimental Systematic Uncertainties

This section describes experimental systematic uncertainties.

11.1. Luminosity and Pile-up

- **luminosity** The preliminary uncertainty on the combined 2015+2016 integrated luminosity is 3.2%. It is derived, following a methodology similar to that detailed in [62], from a preliminary calibration of the luminosity scale using x-y beam-separation scans performed in August 2015 and May 2016[63].
- **pile-up** compute the systematics by changing the nominal data scale of 1.0/1.09 by 1.0/1.0 or 1.0/1.18 to get respectively the up and down variations [64].

11.2. Triggers

11.2.1. $E_{\mathrm{T}}^{\mathrm{miss}}$ trigger

The $E_{\mathrm{T}}^{\mathrm{miss}}$ trigger SF measurement is computed on $W(\mu, \nu)$+jets events. Two effects are taken into account as systematics. First we consider the statistical error the SF as an uncertainty : `METTrigStat`. Then we consider, the difference of SF measurement coming from different physics process. So trigger SF has been measured on $t\bar{t}$ events. The difference of SF($t\bar{t}$) with respect to SF($W(\mu, \nu)$+jets) for a given $E_{\mathrm{T}}^{\mathrm{miss}}$ value is defined as a systematics : `METTrigTop`. Detailed studies and results are in Section 5.1.

11.2.2. Lepton trigger

The lepton trigger systematics are provided by CP groups and links to recommendation can be found in Section 5.2.

The trigger systematics for electron are returned by CP tool as `EL_EFF_Trigger_TotalCorrUncertainty`. It contains the systematics and statistical error on the trigger SF. Systematics is obtained by doing variation of $+/-1$ σ of this error.

For the muons, the CP tool returns two components : the systematics error (`MUON_EFF_TrigSystUncertainty`) and the statistical error (`MUON_EFF_TrigStatUncertainty`) on the trigger SF. Systematics are obtained by doing variation of $+/-1$ σ of these errors.

11.3. Electrons

11.3.1. Electron efficiency systematic

Reconstruction and identification (ID) efficiency and its systematic uncertainties are provided by the CP group as `ElectronEfficiencyCorrection` [17]. The electron efficiency scale factors have been calculated using the full data of 2015 and 2016 13 TeV. The reconstruction efficiency is 97-99% in the entire p_{T} range. The ID efficiency scale factor is available from $p_{\mathrm{T}} > 7$ GeV. The scale factor of the combined cuts of impact parameter significance and on $|z_0 \sin\theta|$ is included in ID efficiency scale factor. The isolation

efficiency scale factor is also provided. In current recommendation scale factors for $p_{\mathrm{T}} > 150$ GeV are unity due to lack of statistics to measure scale factor. Therefore a systematic uncertainty of additional ±2% is assigned above 150 GeV. Three independent systematic sources (`EL_EFF_ID_TotalCorreUncertainty`, `EL_EFF_Reco_TotalCorrUncertainty`, `EL_EFF_Iso_TotalCorrUncertainty`) are considered as electron efficiency systematic uncertainties.

11.3.2. Electron energy scale and resolution

Energy scale and resolution systematic uncertainties have been provided by CP group [65]. More than 60 systematic variation are considered in the energy calibration. However, the electron energy scale and resolution systematic uncertainties are not dominant systematic sources. This analysis is very weekly sensitive to the energy scale and resolution. Therefore, we used simple a systematic model. Two systematic uncertainties (`EG_RESOLUTION_ALL`, `EG_SCALE_ALL`) are considered in this analysis.

11.4. Muons

11.4.1. Muon efficiency systematic uncertainties

Reconstruction, isolation and track-to-vertex association (d_0 significance and $z_0 \sin\theta$) scale factors are calculated using $Z \to \mu\mu$ and $J/\psi \to \mu\mu$ events in the full data of 2015, which corresponds to 3.2 fb^{-1} (`MuonEfficiencyCorrections-03-02-05`) [18]. The scale factor is valid in the full p_{T} range. Since J/ψ measurement is valid below 15 GeV and Z measurement is more accurate above 15 GeV, the separated systeamatic uncertainties are used in low-p_{T} (below 15 GeV). Four independent systematic uncertainties (`MUON_EFF_STAT`, `MUON_EFF_STAT_LOWPT`, `MUON_EFF_SYS`, `MUON_EFF_SYS_LOWPT`) are provided. The isolation scale factor and its systematic uncertainties (`MUON_ISO_STAT`, `MUON_ISO_SYS`) are supported in the range of $10 < p_{\mathrm{T}} < 500$ GeV. For muons out of this range, the scale factor is 1±0.05. The scale factor of the combined cuts on the Impact parameter significance and the $|z_0 \sin\theta|$ is also provided from above MuonEfficiencyCorrections version. Two kinds of independent systematic uncertainties (`MUON_TTVA_STAT`, `MUON_TTVA_SYS`) are provided. Systematic uncertainties are evaluated from $\pm 1\sigma$ variations.

11.4.2. Muon momentum scale and resolution

Muon momentum scale and resolution correction and uncertainties are provided by the CP group (`MuonMomentumCorrections-01-00-29`) [18]. Muons have been calibrated with $Z \to \mu\mu$ for the high p_T region ($p_{\mathrm{T}} > 20$ GeV) and with $J/\psi \to \mu\mu$ for the low p_{T} region ($p_{\mathrm{T}} < 20$ GeV). Three kinds of systematic sources (`MUONS_ID`, `MUONS_MS`, `MUONS_SCALE`) related to scale and resolution are provided. These systematic uncertainties are evaluated by varying the scale and the ID/MS track $\pm 1\sigma$.

11.5. Jets

11.5.1. Regular-*R* Jets

Jet systematics are implemented through the `JetUncertaintiesTool` using the usual PAT interface for systematic variations. The number of uncertainties is divided into different reduction categories. An analysis may choose between the full set of nuisance parameters (~50 baseline parameters) or a globally reduced set of 21 parameters. The baseline set uses *in-situ* analyses, eta intercalibration, high-p_{T} jets, pile-up, flavour composition, flavour response, b-jets, and punch-through jets. Each of these areas of concern may be accessed separately using the tool. The reduced sets comprise nuisance parameters made from performing a principal component analysis and combining the resulting variations in such a way as to preserve correlations in certain jet-kinematic regions. If an analysis will later combine their result with another group, these reduced sets may not be used. We use the 21-parameter reduced set.

The most prominent sources of jet-related uncertainty are the uncertainties from the jet energy scale (JES) and jet energy resolution (JER). The determination of the JES is documented in [66] and the JER is determined from data-MC comparisons. Both uncertainties are available through the `JetUncertaintiesTool`.

No systematic uncertainties associated with the b-jet corrections are found to be necessary, as data and MC agree in a $Z + b$ dataset, as described in Section 7.3.7. For the muon-in-jet correction, the muon p_{T} was changed within its resolution and scale and was shown not to affect $m_{b\bar{b}}$, so no systematic uncertainty was assigned. For the PtReco no systematic uncertainty was assigned *per se*, but the jet p_{T} was changed within its scale and resolution before applying the same PtReco correction and the different $m_{b\bar{b}}$ shapes were used for systematic uncertainties.

11.5.2. Large-*R* Jets

The large-R jet energy scale and resolution uncertainties are evaluated together with the mass and resolution uncertainty. These are named `FATJET_JER`, `FATJET_JMR`, and `FATJET_D2R`. Large-R JES systematic correlation scheme has been tested in various scenarios.

11.6. $E_{\mathrm{T}}^{\mathrm{miss}}$

$E_{\mathrm{T}}^{\mathrm{miss}}$ systematics are implemented through the `METSystematicsTool` using the usual PAT interface. This tool can be configured to account for calorimeter-based jets and track-based jets. The uncertainties related to TST are concerned with MC-to-data disagreements, and thus are not needed when using data. The list of uncertainties associated with $E_{\mathrm{T}}^{\mathrm{miss}}$ in this analysis are `MET_SoftTrk_ResoPara`, `MET_SoftTrk_ResoPerp`, `MET_SoftTrk_ScaleDown`, `MET_SoftTrk_ScaleUp`, `MET_JetTrk_ScaleDown` , and `MET_JetTrk_ScaleUp`.

11.7. Flavour Tagging

The uncertainties related to b-tagging jets are implemented as event-weight systematics (scale factors). These scale factors (SF) are calculated in the following ways:

Reduction Scheme	Number of variations:		
	b-jet	c-jet	light-jet
Medium	3	3	5

Table 14: Flavor tagging reduction schemes. Fewer variations yield a less accurate preservation of total error and correlations. τ-jet variations are identical to c-jet variations with an additional systematic for the c-to-τ extrapolation.

1. For each signal jet identify if it has been b-tagged or not. If it has, multiply the event weight by the SF retrieved from the `BTaggingEfficiencyTool` CP tool. Otherwise, multiply the event weight by the inefficiency SF (InSF) retrieved from the same tool. This will yield the "Nominal" event weight.
2. For each systematic, vary the SF and InSF by the systematic using the `BTaggingEfficiencyTool` and repeat step 1 and store the event weight for this systematic.
3. For all histograms, make a separate histogram for each weight systematic using the corresponding weight.

The individual systematics for b-tagging are on the order of about 40 elements per flavour (b, c, τ, and light). In an effort to alleviate the burden of accounting for ~160 systematics variations the flavour tagging CP group has performed a principal component analysis to reduce the number of systematic variations. This reduction is summarized in Table 14 for the chosen medium (70%) operating point .

Each analysis must determine the appropriate reduction scheme based on the observed effects on the final distributions. There are two additionally systematics that are not part of the reduction scheme and must be treated separately. These are uncertainties related to the p_{T} extrapolation [67] and charm-to-bottom quark extrapolation. A list of the "Medium" systematics include: `FT_EFF_Eigen_Light0`, `FT_EFF_Eigen_Light1`, `FT_EFF_Eigen_Light2`, `FT_EFF_Eigen_Light3`, `FT_EFF_Eigen_Light4`, `FT_EFF_Eigen_B0`, `FT_EFF_Eigen_B1`, `FT_EFF_Eigen_B2`, `FT_EFF_Eigen_C0`, `FT_EFF_Eigen_C1`, `FT_EFF_Eigen_C2`, `FT_EFF_Eigen_extrapolation`,
and `FT_EFF_Eigen_extrapolation_from_charm`.

Additionally, if more than one jet collection is used in b-tagging, each collection will need its own set of systematics. If this is the case, our convention is that the systematic names are postfixed with the jet collection name.

Appendix

In a paper, an appendix is used for technical details that would otherwise disturb the flow of the paper. Such an appendix should be printed before the Bibliography.

A. CP tools used in this analysis

CP tools are based on AnalysisBase 2.4.27.

- `IsolationSelection-00-06-05`
- `PileupReweighting-00-04-01`
- `ReweightUtils-00-03-01`
- `ElectronEfficiencyCorrection-00-01-94`
- `ElectronPhotonFourMomentumCorrection-02-03-00`
- `IsolationCorrections-00-01-27`
- `CalibrationDataInterface-00-05-14`
- `xAODBTaggingEfficiency-00-00-36`
- `MuonEfficiencyCorrections-04-00-11`
- `MuonMomentumCorrections-01-00-60`
- `JetCPInterfaces-00-00-04`
- `JetCalibTools-00-04-76`
- `JetResolution-03-00-49`
- `JetUncertainties-00-09-62`
- `METUtilities-00-02-46`
- `TrigDecisionTool-00-03-55`
- `TrigMuonEfficiency-00-02-47`

B. Trigger list in derivations

MET Triggers	Lepton triggers
HLT_xe35	HLT_e17_lhloose_L1EM15
HLT_xe50	HLT_e24_medium_iloose_L1EM18VH
HLT_xe60	HLT_e24_medium_iloose_L1EM20VH
HLT_xe70	HLT_e24_lhmedium_iloose_L1EM20VH
HLT_xe80	HLT_e24_tight_iloose
HLT_xe80_L1XE50	HLT_e24_lhmedium_L1EM20VHI
HLT_xe80_L1XE70	HLT_e24_lhmedium_L1EM20VH
HLT_xe100	HLT_e24_lhmedium_L1EM18VH
HLT_xe80_tc_lcw_L1XE50	HLT_e24_lhmedium_ivarloose
HLT_xe90_tc_lcw_L1XE50	HLT_e24_lhmedium_nod0_ivarloose
HLT_xe100_tc_lcw_L1XE50	HLT_e24_lhmedium_nod0_L1EM20VH
HLT_xe110_tc_lcw_L1XE60	HLT_e24_lhtight_iloose
HLT_xe80_mht_L1XE50	HLT_e24_lhtight_ivarloose
HLT_xe90_mht_L1XE50	HLT_e24_lhtight_nod0_ivarloose
HLT_xe100_mht_L1XE50	HLT_e26_tight_iloose
HLT_xe100_mht_L1XE60	HLT_e26_tight1_iloose
HLT_xe110_mht_L1XE50	HLT_e26_lhtight_iloose
HLT_xe110_mht_L1XE50_AND_xe70_L1XE50	HLT_e26_lhtight_iloose
HLT_xe130_mht_L1XE50	HLT_e26_lhtight_ivarloose
HLT_xe90_L1XE50	HLT_e26_lhtight_nod0_ivarloose
HLT_xe100_L1XE50	HLT_e26_lhtight_smooth_ivarloose
HLT_xe110_L1XE60	HLT_e60_medium
HLT_xe80_tc_em_L1XE50	HLT_e60_medium1
HLT_xe90_tc_em_L1XE50	HLT_e60_lhmedium
HLT_xe100_tc_em_L1XE50	HLT_e60_lhmedium_nod0
HLT_xe80_tc_lcw	HLT_e120_lhloose
HLT_xe90_tc_lcw	HLT_e140_lhloose
HLT_xe100_tc_lcw	HLT_e140_lhloose_nod0
HLT_xe90_mht	HLT_e300_etcut
HLT_xe100_mht	HLT_mu14
HLT_xe90_tc_lcw_wEFMu_L1XE50	HLT_mu20_iloose_L1MU15
HLT_xe90_mht_wEFMu_L1XE50	HLT_mu20_ivarloose_L1MU15
HLT_xe120_pueta	HLT_mu24_iloose_L1MU15
HLT_xe120_pufit	HLT_mu24_iloose
HLT_xe100_tc_lcw_L1XE60	HLT_mu24_ivarloose
HLT_xe110_tc_em_L1XE50	HLT_mu24_ivarloose_L1MU15
HLT_xe110_tc_em_wEFMu_L1XE50	HLT_mu24_imedium
HLT_xe120_pueta_wEFMu	HLT_mu24_ivarmedium
HLT_xe120_mht	HLT_mu26_imedium
HLT_xe120_tc_lcw	HLT_mu26_ivarmedium
HLT_xe120_mht_wEFMu	HLT_mu40
HLT_xe110_L1XE50	HLT_mu50
HLT_xe100_L1XE60	
HLT_xe120_pufit_wEFMu	
HLT_xe120_tc_lcw_wEFMu	
HLT_xe120_tc_em	

Table 15: Triggers used in Derivation

References

[1] G. Aad et al., *Observation of a new particle in the search for the Standard Model Higgs boson with the ATLAS detector at the LHC*, Phys. Lett. **B716** (2013) 1–29, arXiv: 1207.7214 [hep-ex].

[2] S. Chatrchyan et al., *Observation of a new boson at a mass of 125 GeV with the CMS experiment at the LHC*, Phys. Lett. **B716** (2012) 30–61, arXiv: 1207.7235 [hep-ex].

[3] G. Aad et al., *Combined Measurement of the Higgs Boson Mass in pp Collisions at $\sqrt{s}$ = 7 and 8 TeV with the ATLAS and CMS Experiments*, Phys. Rev. Lett. **114** (2015) 191803, arXiv: 1503.07589 [hep-ex].

[4] 'Measurements of the Higgs boson production and decay rates and constraints on its couplings from a combined ATLAS and CMS analysis of the LHC pp collision data at $\sqrt{s}$ = 7 and 8 TeV', tech. rep. ATLAS-CONF-2015-044, CERN, 2015, URL: http://cds.cern.ch/record/2052552.

[5] G. Aad et al., *Search for the $b\bar{b}$ decay of the Standard Model Higgs boson in associated $(W/Z)H$ production with the ATLAS detector*, JHEP **01** (2015) 069, arXiv: 1409.6212 [hep-ex].

[6] G. Aad et al., *Search for a CP-odd Higgs boson decaying to Zh in pp collisions at $\sqrt{s}$ = 8 TeV with the ATLAS detector*, Phys. Lett. **B744** (2015) 163–183, arXiv: 1502.04478 [hep-ex].

[7] M Baak et al., 'Data Quality Status Flags and Good Run Lists for Physics Analysis in ATLAS', tech. rep. ATL-COM-GEN-2009-015, CERN, 2009, URL: https://cds.cern.ch/record/1168026.

[8] ATLAS Collaboration, *ExtendedPileupReweighting*, https://twiki.cern.ch/twiki/bin/view/AtlasProtected/ExtendedPileupReweighting, 2015, URL: https://twiki.cern.ch/twiki/bin/view/AtlasProtected/ExtendedPileupReweighting (visited on 27/01/2016).

[9] W. Buttinger, 'Using Event Weights to account for differences in Instantaneous Luminosity and Trigger Prescale in Monte Carlo and Data', tech. rep. ATL-COM-SOFT-2015-119, CERN, 2015, URL: https://cds.cern.ch/record/2014726.

[10] ATLAS Collaboration, *Lowest un-prescaled triggers per data-taking period*, https://twiki.cern.ch/twiki/bin/viewauth/Atlas/LowestUnprescaled, 2016, URL: https://twiki.cern.ch/twiki/bin/viewauth/Atlas/LowestUnprescaled (visited on 06/12/2015).

[11] Wei Wang, *MET trigger SF measurement*, https://indico.cern.ch/event/540849/contributions/2225791/attachments/1302560/1945177/METtriggerSF_201607 2016, URL: https://indico.cern.ch/event/540849/contributions/2225791/attachments/1302560/1945177/METtriggerSF_20160701.pdf (visited on 01/07/2016).

[12] Wei Wang, *Update on MET trigger SF measurement*, https://indico.cern.ch/event/603264/contributions/2441464/attachments/1397774/2131542/20170116_met_trigger_ 2017, URL: https://indico.cern.ch/event/603264/contributions/2441464/attachments/1397774/2131542/20170116_met_trigger_SFs.pdf (visited on 18/01/2017).

[13] Alyssa Montalbano, *Trigger sensitivity studies for 1 lepton muon channel*, https://indico.cern.ch/event/609432/contributions/2457202/attachments/1403815/2144084/triggerStudiesUpdate.pd 2017, URL: https://indico.cern.ch/event/609432/contributions/2457202/attachments/1403815/2144084/triggerStudiesUpdate.pdf (visited on 30/01/2017).

[14] Yanhui Ma, *Trigger study for VHbb 1-lepton channel*, https://indico.cern.ch/event/609432/contributions/2457201/attachments/1403801/2143935/VHbb_1lepton_201701 2017, URL: https://indico.cern.ch/event/609432/contributions/2457201/attachments/1403801/2143935/VHbb_1lepton_20170130.pdf (visited on 30/01/2017).

[15] ATLAS Collaboration, *Muon Trigger Public Results*, https://twiki.cern.ch/twiki/bin/view/AtlasPublic/MuonTriggerPublicResults, 2016, URL: https://twiki.cern.ch/twiki/bin/view/AtlasPublic/MuonTriggerPublicResults.

[16] ATLAS Collaboration, *Public Egamma Trigger Plots for Collision Data*, https://twiki.cern.ch/twiki/bin/view/AtlasPublic/EgammaTriggerPublicResults, 2016, URL: https://twiki.cern.ch/twiki/bin/view/AtlasPublic/EgammaTriggerPublicResults.

[17] ATLAS Collaboration, *Electron Efficiencies for Run2 (scale factors and uncertainties)*, https://twiki.cern.ch/twiki/bin/viewauth/AtlasProtected/ElectronEfficiencyRun2, 2015, URL: https://twiki.cern.ch/twiki/bin/viewauth/AtlasProtected/ElectronEfficiencyRun2 (visited on 09/12/2016).

[18] ATLAS Collaboration, *MCPAnalysisGuidelinesMC15*, https://twiki.cern.ch/twiki/bin/view/AtlasProtected/MCPAnalysisGuidelinesMC15, 2015, URL: https://twiki.cern.ch/twiki/bin/view/AtlasProtected/MCPAnalysisGuidelinesMC15 (visited on 31/10/2015).

[19] Chikuma Kato, *Lepton Trigger Efficiency*, https://indico.cern.ch/event/390200/session/0/attachments/780748/1700642/20151022_ckato_lepton_trigger.pdf, 2015, URL: https://indico.cern.ch/event/390200/session/0/attachments/780748/1700642/20151022_ckato_lepton_trigger.pdf (visited on 21/10/2015).

[20] Chikuma Kato, *Lepton Trigger*, https://indico.cern.ch/event/532658/contributions/2171183/attachments/1274821/1894630/slides.pdf, 2016, URL: https://indico.cern.ch/event/532658/contributions/2171183/attachments/1274821/1894630/slides.pdf (visited on 18/05/2016).

[21] Tatsuya Masubuchi, *Trigger Option for VH 2lep*, https://indico.cern.ch/event/540849/contributions/2400151/attachments/1384373/2105950/VHtrigger.pdf, 2016, URL: https://indico.cern.ch/event/540849/contributions/2400151/attachments/1384373/2105950/VHtrigger.pdf (visited on 07/12/2016).

[22] M Delmastro et al., 'Photon identification efficiency measurements with the ATLAS detector using LHC Run 1 data', tech. rep. ATL-COM-PHYS-2014-949, CERN, 2014, URL: https://cds.cern.ch/record/1747242.

[23] 'Improved electron reconstruction in ATLAS using the Gaussian Sum Filter-based model for bremsstrahlung', tech. rep. ATLAS-CONF-2012-047, CERN, 2012, URL: https://cds.cern.ch/record/1449796.

[24] 'Electron efficiency measurements with the ATLAS detector using the 2012 LHC proton-proton collision data', tech. rep. ATLAS-CONF-2014-032, CERN, 2014, URL: https://cds.cern.ch/record/1706245.

[25] ATLAS Collaboration, *Electron and Photon Selection and Identification for Run2*, https://twiki.cern.ch/twiki/bin/view/AtlasProtected/EGammaIdentificationRun2, 2015, URL: https://twiki.cern.ch/twiki/bin/view/AtlasProtected/EGammaIdentificationRun2 (visited on 06/02/2017).

[26] ATLAS Collaboration, *Official Isolation Working Points*, https://twiki.cern.ch/twiki/bin/view/AtlasProtected/IsolationSelectionTool, 2015, URL: https://twiki.cern.ch/twiki/bin/view/AtlasProtected/IsolationSelectionTool (visited on 17/01/2017).

[27] G. Aad et al., *Measurement of the muon reconstruction performance of the ATLAS detector using 2011 and 2012 LHC proton–proton collision data*, Eur. Phys. J. **C74**.11 (2014) 3130, arXiv: 1407.3935 [hep-ex].

[28] ATLAS Collaboration, *Unified Muon Identification Chain*, https://twiki.cern.ch/twiki/bin/view/AtlasProtected/MuonsCollection, 2015, URL: https://twiki.cern.ch/twiki/bin/view/AtlasProtected/MuonsCollection (visited on 19/11/2015).

[29] 'Muon reconstruction performance in early $\sqrt{s}$=13 TeV data', tech. rep. ATL-PHYS-PUB-2015-037, CERN, 2015, URL: https://cds.cern.ch/record/2047831.

[30] ATLAS Collaboration, *MuonSelectionTool*, https://twiki.cern.ch/twiki/bin/view/Atlas/MuonSelectionTool, 2015, URL: https://twiki.cern.ch/twiki/bin/view/Atlas/MuonSelectionTool (visited on 09/12/2015).

[31] ATLAS Collaboration, *Tracking CP Recommendations for the End Of Year Event 2015*, https://twiki.cern.ch/twiki/bin/view/AtlasProtected/TrackingCPEOYE2015, 2015, URL: https://twiki.cern.ch/twiki/bin/view/AtlasProtected/TrackingCPEOYE2015 (visited on 19/11/2015).

[32] *Run II b-jet energy correction in VH* (), URL: https://twiki.cern.ch/twiki/bin/viewauth/AtlasProtected/HSG5BJetEnergyCorr.

[33] 'Reconstruction, Energy Calibration, and Identification of Hadronically Decaying Tau Leptons in the ATLAS Experiment for Run-2 of the LHC', tech. rep. ATL-PHYS-PUB-2015-045, CERN, 2015, URL: https://cds.cern.ch/record/2064383.

[34] ATLAS Collaboration, *2015 Tau Recommendations*, https://twiki.cern.ch/twiki/bin/view/AtlasProtected/TauPreRecommendations2015, 2015, URL: https://twiki.cern.ch/twiki/bin/view/AtlasProtected/TauPreRecommendations2015 (visited on 07/06/2016).

[35] ATLAS Collaboration, *2016 Tau Recommendations*, https://twiki.cern.ch/twiki/bin/view/AtlasProtected/TauRecommendationsSummer2016, 2016, URL: https://twiki.cern.ch/twiki/bin/view/AtlasProtected/TauRecommendationsSummer2016 (visited on 18/07/2016).

[36] W Lampl et al., 'Calorimeter Clustering Algorithms: Description and Performance', tech. rep. ATL-LARG-PUB-2008-002. ATL-COM-LARG-2008-003, CERN, 2008, URL: https://cds.cern.ch/record/1099735.

[37] M. Cacciari, G. P. Salam and G. Soyez, *The anti-k_t jet clustering algorithm*, Journal of High Energy Physics **2008**.04 (2008) 063, URL: http://stacks.iop.org/1126-6708/2008/i=04/a=063.

[38] ATLAS Collaboration, 'Tagging and suppression of pileup jets with the ATLAS detector', tech. rep. ATLAS-CONF-2014-018, CERN, 2014, URL: https://cds.cern.ch/record/1700870.

[39] ATLAS Collaboration, 'Expected performance of the ATLAS *b*-tagging algorithms in Run-2', tech. rep. ATL-PHYS-PUB-2015-022, CERN, 2015, URL: https://cds.cern.ch/record/2037697.

[40] ATLAS Collaboration, *BTaggingTwiki*, https://twiki.cern.ch/twiki/bin/view/AtlasProtected/BTagCalib2015#Recommendation_June_2017, 2017, URL: https://twiki.cern.ch/twiki/bin/view/AtlasProtected/BTagCalib2015#Recommendation_June_2017 (visited on 08/06/2017).

[41] *Data-driven determination of the energy scale and resolution of jets reconstructed in the ATLAS calorimeters using dijet and multijet events at sqrt(s)=8 TeV*, ATLAS-CONF-2015-017 (2015), URL: http://cdsweb.cern.ch/record/2008678.

[42] *Jet global sequential corrections with the ATLAS detector in proton-proton collisions at sqrt(s) = 8 TeV*, ATLAS-CONF-2015-002 (2015), URL: http://cdsweb.cern.ch/record/2001682.

[43] ATLAS Collaboration, 'Search for a Standard Model Higgs boson produced in association with a vector boson and decaying to a pair of b-quarks', tech. rep. ATL-COM-PHYS-2016-1724, CERN, 2016, URL: https://cds.cern.ch/record/2235437.

[44] *Search for the $b\bar{b}$ decay of the Standard Model Higgs boson in associated $(W/Z)H$ production with the ATLAS detector*, accepted for publication by JHEP (2014), arXiv: 1409.6212 [hep-ex].

[45] T. Aaltonen et al., *Improved b-jet energy correction for $H \to b\bar{b}$ searches at CDF*, submitted to Nucl. Instrum. Meth. (2011), arXiv: 1107.3026 [hep-ex].

[46] T. Aaltonen et al., *Search for the standard model Higgs boson decaying to a bb pair in events with one charged lepton and large missing transverse energy using the full CDF data set*, Phys.Rev.Lett. **109** (2012) 111804, arXiv: 1207.1703 [hep-ex].

[47] S. Chatrchyan et al., *Search for the standard model Higgs boson produced in association with a W or a Z boson and decaying to bottom quarks*, Phys.Rev. **D89**.1 (2014) 012003, arXiv: 1310.3687 [hep-ex].

[48] V. Khachatryan et al., *Search for the standard model Higgs boson produced through vector boson fusion and decaying to $b\bar{b}$*, Phys. Rev. **D92**.3 (2015) 032008, arXiv: 1506.01010 [hep-ex].

[49] *Impact of jet-energy corrections on the ATLAS Run I $WH \to l\nu b\bar{b}$ search*, ATL-PHYS-INT-2015-004 (2015), URL: https://cds.cern.ch/record/1982455.

[50] E. Schopf, 'Improvement of the Mass Resolution in the $H \to b\bar{b}$ Decay Using Multivariate Regression in ATLAS Data', tech. rep. BONN-IB-2014-07, Physikalisches Institut Bonn, 2014.

[51] T. Masubuchi, D. O. Jamin and J. W. Hetherly, 'Object selections for the SM VH and $A \to Zh$ search with V decaying leptonically and $H \to b\bar{b}$ with Run-2 data collected with the ATLAS detector at $\sqrt{s}$ = 13 TeV - Supporting Document -', tech. rep. ATL-COM-PHYS-2015-1467, ATLAS, 2015, URL: https://cds.cern.ch/record/2110713.

[52] Kevin Mercurio, *Validation of the b-jet Jet Energy Scale Using In-Situ Techniques in 2011*, https://indico.cern.ch/event/194205/contributions/1472068/subcontributions/133320/attachments/281167/39314 10-02.pdf, 2011, URL: https://indico.cern.ch/event/194205/contributions/1472068/subcontributions/133320/attachments/281167/393144/BjetJES_Balance2012-10-02.pdf (visited on 16/01/2016).

[53] K. Olive et al., *Review of Particle Physics*, Chin.Phys. **C38** (2014) 090001.

[54] Naoki Ishijima, *Validation of b-jet correction in Z + b process*, https://indico.cern.ch/event/606694/contributions/2446444/attachments/1399365/2136736/Hbb_ishijima_2017011 2017, URL: https://indico.cern.ch/event/606694/contributions/2446444/attachments/1399365/2136736/Hbb_ishijima_20170115.pdf (visited on 16/01/2016).

[55] ATLAS Collaboration, 'Jet mass reconstruction with the ATLAS Detector in early Run 2 data', tech. rep. ATLAS-CONF-2016-035, CERN, 2016, URL: https://cds.cern.ch/record/2200211.

[56] Chikuma Kato, *PtReco Correction*, https://indico.cern.ch/event/390200/contribution/52/attachments/1172417/1751301/20151131_ckato_ptreco.pdf, 2016, URL: https://indico.cern.ch/event/390200/contribution/52/attachments/1172417/1751301/20151131_ckato_ptreco.pdf (visited on 31/11/2015).

[57] 'Recommendations of the Physics Objects and Analysis Harmonisation Study Groups 2014.', tech. rep. ATL-PHYS-INT-2014-018, CERN, 2014, URL: https://cds.cern.ch/record/1743654.

[58] Will Buttinger, *Updated Overlap Removal Working Points*, https://indico.cern.ch/event/457238/, 2015, URL: https://indico.cern.ch/event/457238/ (visited on 16/12/2015).

[59] Kristian Gregersen, *Overlap Removal in CxAODFramework*, https://indico.cern.ch/event/484076/contributions/2002277/attachments/1244080/1831206/Overlap_removal_in_C 2016, URL: https://indico.cern.ch/event/484076/contributions/2002277/attachments/1244080/1831206/Overlap_removal_in_CxAODFramework.pdf (visited on 30/03/2016).

[60] ATLAS Collaboration, 'Performance of missing transverse momentum reconstruction for the ATLAS detector in the first proton-proton collisions at at $\sqrt{s}$= 13 TeV', tech. rep. ATL-PHYS-PUB-2015-027, CERN, 2015, URL: https://cds.cern.ch/record/2037904.

[61] ATLAS Collaboration, *Usage of Missing ET in analyses: rebuilding and systematics*, https://twiki.cern.ch/twiki/bin/viewauth/AtlasProtected/METUtilities, 2015, URL: https://twiki.cern.ch/twiki/bin/viewauth/AtlasProtected/METUtilities (visited on 12/10/2015).

[62] A. Collaboration, *Luminosity Determination in pp Collisions at sqrt(s) = 8 TeV using the ATLAS Detector at the LHC*, Eur. Phys. J. C **76** (2016) 653, arXiv: 1608.03953 [hep-ex].

[63] ATLAS Collaboration, *LuminosityForPhysics*, https://twiki.cern.ch/twiki/bin/view/Atlas/LuminosityForPhysics, 2015, URL: https://twiki.cern.ch/twiki/bin/view/Atlas/LuminosityForPhysics (visited on 03/12/2015).

[64] ATLAS Collaboration, *ExtendedPileupReweighting*, https://twiki.cern.ch/twiki/bin/view/AtlasProtected/ExtendedPileupReweighting, 2015, URL: https://twiki.cern.ch/twiki/bin/view/AtlasProtected/ExtendedPileupReweighting (visited on 30/11/2015).

[65] ATLAS Collaboration, *Electron and Photon Calibration for Run2 (energy scale and resolution)*, https://twiki.cern.ch/twiki/bin/view/AtlasProtected/EGammaCalibrationRun2, 2015, URL: https://twiki.cern.ch/twiki/bin/view/AtlasProtected/EGammaCalibrationRun2 (visited on 02/12/2016).

[66] 'Jet Calibration and Systematic Uncertainties for Jets Reconstructed in the ATLAS Detector at $\sqrt{s}$ = 13 TeV', tech. rep. ATL-PHYS-PUB-2015-015, CERN, 2015, URL: https://cds.cern.ch/record/2037613.

[67] G. Watts, F. Filthaut and G. Piacquadio, 'Extrapolating Errors for *b*-tagging', tech. rep. ATL-COM-PHYS-2015-711, This is for internal information only, no approval to ever be seen outside of ATLAS.: CERN, 2015, URL: https://cds.cern.ch/record/2034234.

List of contributions

Ahmadov, Faig	1-lepton analyzer, MVA and statistical analysis
Argyropoulos, Spyridon	MC contact, CxAOD framework, Study of systematics smoothing
Arnold, Hannah	CxAOD framework
Amaral Coutinho, Yara	jet resolution studies
Sanchez Pineda, Arturo Rodolfo	CxAOD framework
Bell, Andrew Stuart	1-lepton analyzer, primary input producer, MVA studies, main support note editor, BG modeling, Statistical analysis, Flavour tagging contact
Benitez, Jose	0-lepton analyzer, Main support note editor
Buzatu, Adrian	dijet mass reconstruction, CxAOD framework, Objects support note editor
Calderini, Giovanni	Supervision, BG modeling
Chan, Stephen Kam-wah	Statistical analysis
Chen, Chunhui	Supervision
Buckley, Andrew	Supervision
Buscher, Daniel	BG modelling, CxAOD framework, statistical analysis
Delporte, Charles	0-lepton analyzer, b-tagging studies
De Lorenzi, Francesco	VH boosted studies, statistical analysis
De Vivie De Regie, Jean-Baptiste	Supervision
Dao, Valerio	Coordination of modelling studies, statistical analysis
Enari, Yuji	Supervision
Francavilla, Paolo	BG modeling, Statistical analysis, paper editor
Gargiulo, Simona	W+jets modelling uncertainties
Gaycken, Goetz	Supervision
Gray, Chloe	Signal modelling uncertainties
Grivaz, Jean-Francois	Supervision, analysis review
Hays, Jonathan Michael	CxAOD framework coordinator
Hesketh, Gavin Grant	Supervision
Hobbs, John	Supervision
Huth, John	Supervision
Ishijima, Naoki	1-lepton analyzer, multijet studies
Kado, Marumi	Supervision
Kato, Chikuma	dijet mass reconstruction, CxAOD production
Li, Changqiao	0-lepton analyzer, primary input producer, CxAOD production, statistical analysis
Li, Haifeng	Diboson modelling uncertainties, statistical analysis
Liu, Yanwen	Supervision
Marchiori, Giovanni	Egamma contact, Supervision
Ma, Lianliang	Supervison
Ma, Yanhui	1-lepton analyzer, CxAOD framework, multijet studies
Mario Jose da Cunha Sargedas de Sousa	Statistical analysis
Masubuchi, Tatsuya	2-lepton analyzer, BG modelling, Main supporting note editor
Mallik, Usha	Supervision
Mehta, Andrew	2-lepton analyzer, primary input producer, BG modelling, statistical analysis
Montalbano, Alyssa	1-lepton analyzer, multijet studies, statistical analysis
Morange, Nicolas	Coordination
Moser, Brian	BG modelling
Pandini, Carlo Enrico	0-lepton analyzer, BG and signal modelling
Piacquadio, Giacinto	Paper editor, coordination of multijet studies

1175